Double Muon Trigger Rates in CMS Experiment

Andrzej Fengler

Warsaw 1996

M.Sc. thesis written under supervision of
prof. dr hab. J.Królikowski
from Division of Particles and Fundamental Interactions,
Institute of Experimental Physics,
Warsaw University

Abstract

The main goal of this thesis was to answer the question about 2μ rates expected in the CMS detector. Sources of these rates have been discussed. Influence of chosen detector segmentation on loses of physically interesting events has also been considered. Besides, these simulation studies have examined very preliminary trigger algorithm implemented in current version of CMSIM (CMS simulation package) and revealed some aspects of its operation which should be corrected in future.

Contents

1 Introduction

1.1 Basic informations about LHC

Compact Muon Solenoid (CMS) will be one of two big experiments operating on Large Hadron Collider (LHC) in CERN[1]. It will probably start running in 2005. In LHC which is planed to be placed in the LEP tunnel, protons[2] will be brought to collision at centre of mass energy of 14 TeV[3]. Some basic parameters of LHC operating in p-p mode are given in Table 1 based on [3, pages 5&168].

1.2 Physics motivations

1.2.1 Hunting of Higgs in SM and MSSM

Large energy and very high luminosity are needed if one try to reveal nature of the spontaneous symmetry breaking mechanism in electroweak sector of the Standard Model (SM) due to which particles gain masses. It is expected that the last missing item of the SM – Higgs boson responsible for this process – will be found and its properties precisely measured. The detection range extends from 80–90 GeV/c^2 being LEP II discovery limit to about 1 TeV/c^2 (typical energy of collision constituents). Higgs with higher mass will be very difficult to discover because its width grows rapidly with mass – $\Gamma_H \propto m_H^3$. For example 1 TeV Higgs particle has 0.5 TeV/c^2 width. There are also some theoretical arguments for expecting the Higgs mass bellow 1 TeV. For heavier Higgs, perturbation theory breaks – some couplings become too strong. Depending on Higgs mass different decay channels are used in the detection, optimising on signal to background ratio [4,

[1] The second one will be ATLAS.

[2] Protons were chosen, instead of e^- and e^+ used in LEP, due to smaller synchrotron radiation for them. Power lost by charge particle in a circular accelerator is given by formula $P = \frac{2}{3}\frac{e^2 c}{\rho^2}\beta^4\gamma^4$ [1, pages 632-633] thus a proton with the same energy as electron loses $\frac{m_p^4}{m_e^4} \simeq 10^{13}$ times less energy due to this process. Synchrotron radiation is the most important limitation imposed on $e^- e^+$ colliders.

[3] Nowadays the largest accessible energy in c.m.s. is reached in Tevatron($p\overline{p}$ collider in Fermilab, USA) – E_{cms}=1.8 TeV. Luminosity of this machine was $L = 10^{31}\mathrm{cm}^{-2}\mathrm{s}^{-1}$ in 1994 which is order of magnitude smaller than LHC luminosity at the beginning of operation. Construction of another large future accelerator SSC (Texas,USA) which was expected to collide protons at even more impressive energy – 40 TeV – with designed luminosity $L = 10^{33}\mathrm{cm}^{-2}\mathrm{s}^{-1}$ was unfortunately stopped by US Congress [2, page 124].

Beam energy	7.0	TeV
Relativistic factor γ	7461	
Dipole field	8.4	T
Injection energy	450	GeV
Expected luminosity	10^{34}	$cm^{-2}s^{-1}$
Crossing points	4	
Circulating current/beam	0.536	A
Bunch separation	25	ns
Bunch spacing	7.48	m
Particles per bunch	10^{11}	
Stored energy per beam	334	MJ
Horizontal beam size in arc	0.303	mm
Vertical beam size in arc	0.303	mm
R.M.S bunch length	0.257	ns
R.M.S bunch length	7.7	cm
R.M.S x,y beam size at IP	15.9	μm
Crossing angle at IP	200	μrad
Beam lifetime	22	h
Luminosity lifetime	10	h
Energy loss per turn	6.71	keV

Table 1: LHC parameters

pages 178-188]

- $H \to \gamma\gamma$ for $80 \leq m_H \leq 130$ GeV/c^2
- $H \to ZZ^* \to 2l^+2l^-$ for 130 GeV/c$^2 \leq m_H \leq 2m_Z$
- $H \to ZZ \to 2l^+2l^-$ for $2m_Z \leq m_H \leq$800 GeV/c^2
- $H \to ZZ \to ll\nu\nu$ for $500 \leq m_H \leq$1000 GeV/c^2
- $H \to ZZ \to lljj$ for $m_H \approx$1000 GeV/c^2
- $H \to WW \to l\nu jj$ for $m_H \approx$1000 GeV/c^2

Essentially the same decay channels can be used searching for Minimal Supersymmetric Standard Model (MSSM) Higgs $H^{\pm}$,h,H,A in wide range of two parameters – m_A and $tan\beta$ – which express Higgs boson masses and couplings . Of course production rates are in this case significantly different due to another couplings. Additionally channels

- $h, H, A \ \to \mu^+\mu^-$
- $H^{\pm} \ \to \tau\nu_\tau$

can be explored. The first one is not so much dominated by Drell-Yan background (γ^*, Z

$\rightarrow \mu^+\mu^-$) as in the case of SM Higgs, though the branching ratio for $H \rightarrow \mu^+\mu^-$ is small in both cases $\approx 3 \times 10^{-4}$. The second one $H^\pm$ is chosen because of large $BR(H^\pm \rightarrow \tau\nu_\tau) \approx 98$ %, for $tan\beta > 2$, with weak dependence on $tan\beta$.

1.2.2 SUSY and new gauge bosons

It is expected that at energies exceeding 1 TeV per constituent, completely new set of particles, called SUSY[4] because of being partners of already discovered, can appear. It could help us to answer the question about the dominance of matter under antimatter in our world and reasons of breaking balance. May be new heavy gauge bosons(W',Z',ρ_{TC}) will manifest their presence. In all this scenarios large number of signatures involves presence of several jets at high p_t (excess of b-jets), missing transverse energy and multileptons in final state.

1.2.3 Top and beauty physics

In the first phase of LHC operation at lower luminosity (10^{32} cm^{-2}s^{-1}) it is planned to study heavy flavour (b,t quark) physics. Mass and decay properties of top quark, recently discovered in Tevatron, should be quickly measured due to copious production of $t\bar{t}$ pairs. We will trigger on the isolated lepton (μ, e) from one t decay and study products of the second one. LHC will also provide us with very good possibility to study CP violation in B mesons system[5] which leads to:

$$\Gamma(B^0 \rightarrow f) \neq \Gamma(\overline{B}^0 \rightarrow \overline{f}) \tag{1}$$

The theoretical predictions are reliable only for class of decays to CP eigenstates. Because of small branching ratios ($10^{-4} - 10^{-7}$) for useful decay channels, the huge statistic is essential. There will be $10^{12} - 10^{13}$ $b\bar{b}$ produced per year [4, page 198]. The decay rate asymmetry A in the case of CP states depends only on angle from unitarity triangle ($\theta := \alpha, \beta, \gamma$) :

$$A = \frac{\Gamma(B^0 \rightarrow f) - \Gamma(\overline{B}^0 \rightarrow \overline{f})}{\Gamma(B^0 \rightarrow f) + \Gamma(\overline{B}^0 \rightarrow \overline{f})} \propto \sin 2\theta \tag{2}$$

Especially promising is the measurement of β angle in the $B_d^0 \rightarrow J/\psi K_s^0$ channel. It will be necessary to measure $\mu^+\mu^-$ from J/Ψ decay and $\pi^+\pi^-$ from K_s^0. Additionally tagging of the associated b–hadron decaying into μ + *anything* will be required[6].

[4]SUperSYmmetry particles – squarks,gluinos,sleptons, higsinos,winos and zinos.

[5]In addition to general purpose experiments ATLAS and CMS, *LHC-B* experiment dedicated to B-physics is being considered.

[6]Before trigger-acceptance and cuts the number of signal events will be 5.6×10^6 for integrated luminosity 10^4 pb^{-1}. The uncertainty of this number is very large because of QCD estimation of $\sigma_{b\bar{b}}$ from 0.1 to 0.7 mb for $\sqrt{s} = 14TeV$.

1.2.4 Heavy ion physics

Apart from p-p option, LHC will be used as heavy ion collider (the heaviest Pb-Pb). Centre of mass energy will reach 1150 TeV which comes from 7.0 TeV per charge (2.76 TeV/u i.e. 5.52 TeV per nucleon pair). The highest designed luminosity will exceed $10^{27}\mathrm{cm}^{-2}\mathrm{s}^{-1}$. The bunch spacing will be 125 ns – multiple of 25 ns for protons – to use compatible beam diagnostic electronics and triggers in both modes of operation. It is expected that achieved energy density will be well above the threshold for formation of completely new state of matter – Quark Gluon Plasma (QGP)[7]. One of predicted signatures for QGP is suppression of all heavy quark bound states production with exception for $\Upsilon(1S)$. The reason for this is colour screening. It is planned to examine $\mu^+\mu^-$ rates in Υ family – the ratio of $\Upsilon(2S)$ and $\Upsilon(3S)$ to $\Upsilon(1S)$. We expect suppression for ion collisions relative to pp mode.

1.3 CMS detector

To meet all these requirements completely new detectors – larger than presently existing and based on the latest technical achievements – will be build. One of the two general purpose, high luminosity will be CMS detector, which three dimensional, transverse and longitudinal view (exactly $\frac{1}{4}$) are shown on Fig. 1, 2 and 3 respectively. Total weight will be 14,500 tones and overall cost about 460 Mln CHF [4, page 245].

1.3.1 The tracker

CMS concepts are typical for HEP detectors. Going from the vertex we will meet inner tracker (up to 1.310 m in r and 3.00 m in z). It will be used for precise measurement of momentum and track reconstruction. Silicon pixel detectors will be mounted around the beam pipe. Two layers for barrel and three for endcaps will ensure good vertex detection and flavour tagging. Precision in providing three dimensional space points (15 μm in r,ϕ and 11-90 μm in z) will make allocation of secondary vertex easy even if very close to the primary one. The intermediate tracking volume will be used by microstrip detectors with good spatial (15 μm in r,ϕ and 1 mm in z) and time resolution. Radiation hardness is also sufficient. The outer part of tracker will be equipped with microstrip gas chambers (MSGC), which providing fast charge collection, ensure good time resolution. Spatial resolution will be kept on the level of 40 μm in r,ϕ and 2 mm in z.

1.3.2 The electromagnetic calorimeter

Around the tracker, the electromagnetic calorimeter (EB,EF) will be situated. It will be a crystal calorimeter built of lead tungstate – $PbWO_4$. Good energy resolution of ECAL will be crucial for light Higgs detection thanks to 2γ decay. The design parameters of the

[7]Experiment probing this region of physics is called A Large Ion Collider Experiment (ALICE).

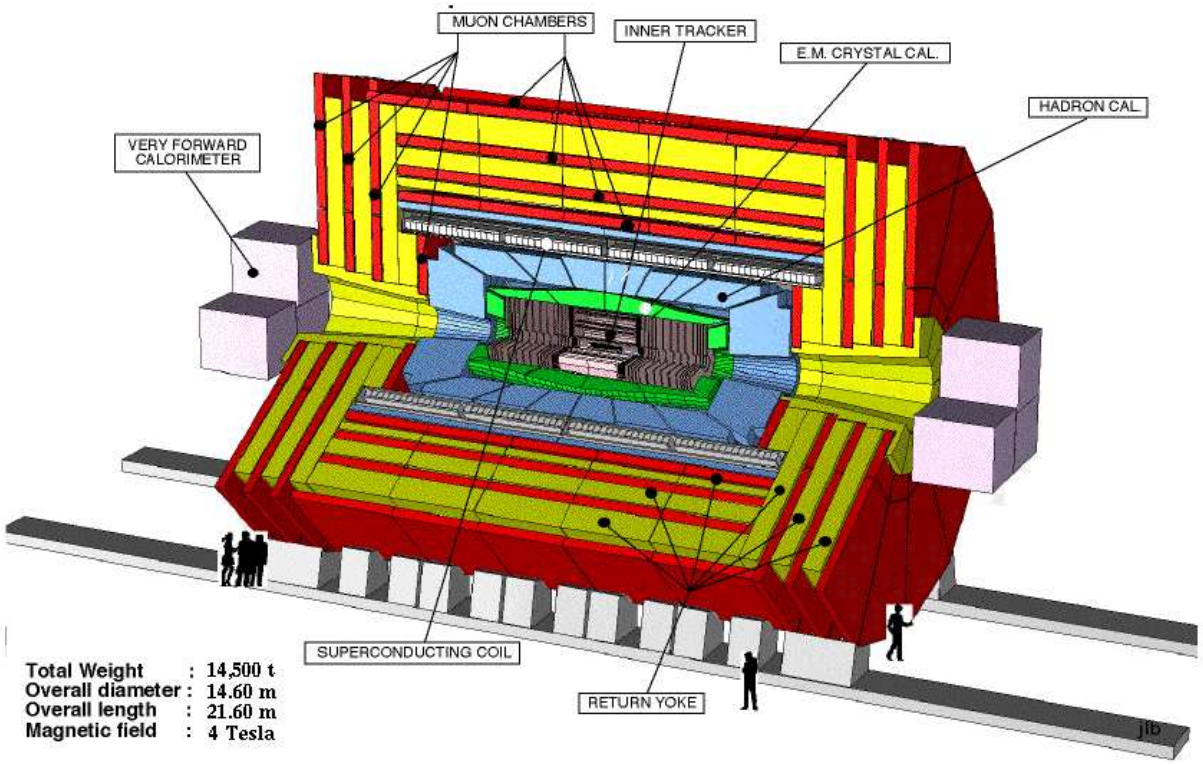

Figure 1: 3D view of the CMS detector

$PbWO_4$ ECAL [4, pages 49–51], result in the following mass resolution for 100 GeV Higgs reconstructed in $H \rightarrow \gamma\gamma$ channel

- 475 MeV for $L = 10^{33}\text{cm}^{-2}\text{s}^{-1}$
- 775 MeV for $L = 10^{34}\text{cm}^{-2}\text{s}^{-1}$

1.3.3 The hadron calorimeter

The next detector element - see Fig. 1 and 3 to locate it – will be hadron calorimeter (HCAL), which in combination with ECAL, has to measure energies and direction of particle jets and to be maximally hermetic to give reliable information about missing transverse energy. HCAL will cover pseudorapidity region up to 3.0 η[8] units in the barrel and endcaps.

The $3.0 < \eta < 5.0$ range will be covered by another calorimeter called very forward (VF). It will help us in top quark and Higgs studies for $m_H > 500$ GeV by detection of two forward tagging jets. Due to large radiation quartz fibres, embedded in copper or iron absorber material, were chosen to ensure high resistance. Light in quartz fibres is generated by the Cherenkov effect therefore it is insensitive to low energy neutrons traversing in large numbers.

[8] $\eta = -ln\, tan\frac{\theta}{2}$.

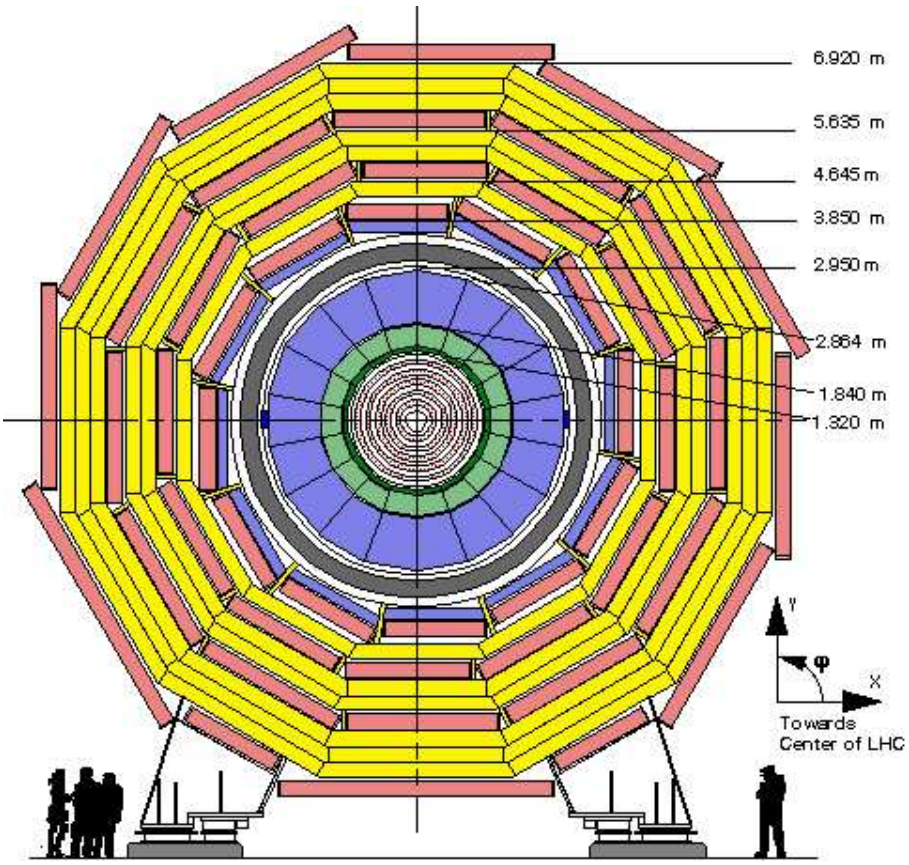

Figure 2: Transverse view of the CMS detector

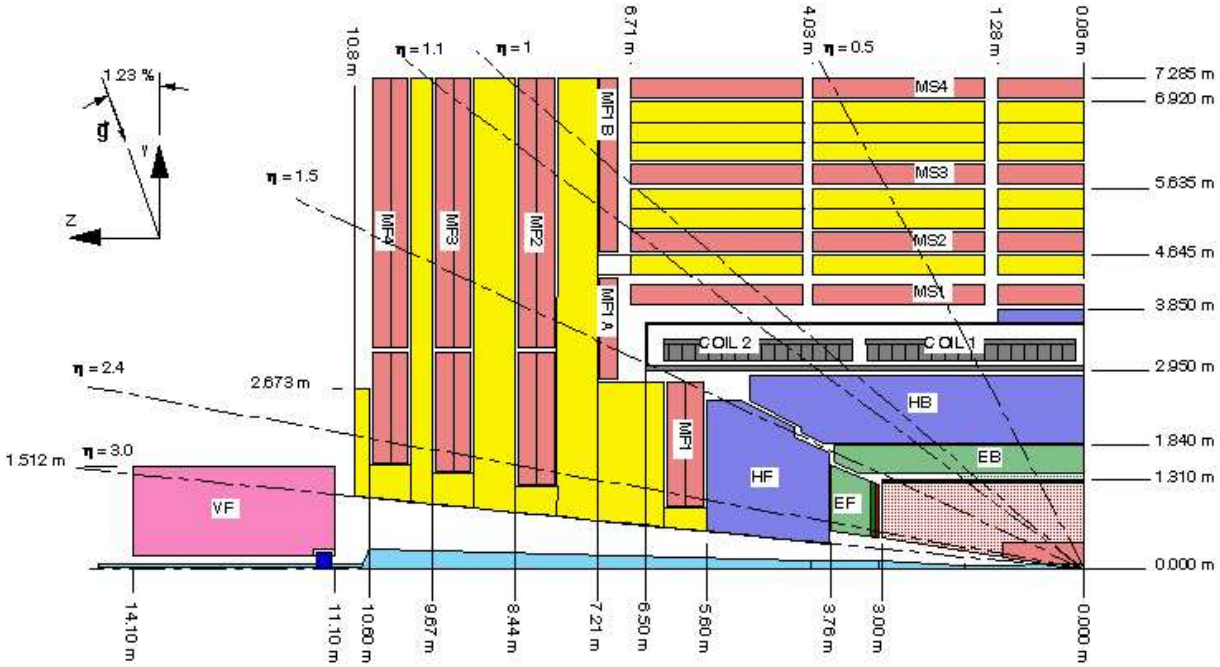

Figure 3: Longitudinal view of the CMS detector

The HCAL in barrel and endcaps will be built of plastic scintillator layers alternated with copper ones. For single hadrons it will have sufficient energy resolution :

$$\frac{\sigma_E}{E} = \frac{65\%}{\sqrt{E}} \oplus 5\% \tag{3}$$

Additionally in the central region HCAL will be assisted by 'tail catcher' which will be situated outside the coil.

1.3.4 The magnet

In the CMS detector, the 4 T[9] magnetic field will be produced by superconducting solenoid of 13 m length and inner diameter of 5.9 m . The choice of solenoid allows muon detection in a wide pseudorapidity region – up to 2.4. The magnetic flux will be returning through 1.8 m thick saturated iron yoke – on Fig. 3 it is yellow. Total iron mass is estimated to be about 11500 tones. Yoke will be divided into five mobile wheels. Apart from closing magnetic field, yoke absorbs remnants of the hadron cascades which leaked from calorimeters, acting as a muon filter.

1.3.5 The muon detector

As one can deduce from section 1.2 the muon detection is crucial for most channels being in our interest – from b and t quark physics, through Higgs with it decays to Z or W subsequently decaying into muons, to SUSY particles. Fig. 2 and 3 present the muon detector system composed of 4 layers. It will cover pseudorapidity region up to $|\eta| = 2.4$[10] and will be placed behind the coil and the calorimeters. In connection with high magnetic field and at least 8.96 λ_I [11] of material for all angles it should assure muon identification, its momentum measurement and trigger. The list of its most important features:

1. transverse momentum resolution for $0 < |\eta| < 2$ – $\Delta p_t/p \simeq$ 6–10% for $p_t = 10$ GeV, 7–20% for $p_t = 100$ GeV and 15–35% for $p_t = 1$ TeV,
2. charge assignment correctness at 99% confidence level upto the highest kinematicaly available momenta,
3. beam crossing tagging with efficiency above 99%,
4. trigger with a variable p_t thresholds from a few GeV to 100 GeV.

Three types of detectors have been chosen – drift tubes (DT), cathode strip chambers (CSC) and resistive plate chambers (RPC) [4, page 93]. DT[12] will be placed only in the

[9] Inside the coil.

[10] It corresponds to polar angles from 9.6 to 170.4 degrees.

[11] Interaction length. There will be 1.1 λ_I coming from the EM, 5.46 λ_I from the HCAL, 1.1 λ_I from the COIL and 1.3 λ_I from TC (Tail Catcher) for $\eta = 0$ in front of the MS1.

[12] Each module consists of twelve planar layers eight parallel and four perpendicular to the beam.

barrel (4 modules – one in each MS1–MS4)[13] where rates will be low (<10 Hz/cm^2). In the endcaps (MF1–MF4), where high magnetic field and rates will be present, CSC[14] were chosen. DT and CSC are able to identify bunch crossing and provide spatial informations. RPC detectors[15] will be placed both in the barrel and the endcaps up to $|\eta| < 2.1$ with the room left up to $|\eta| < 2.4$ for the future upgrade. Due to the short reaction time RPC will be used for trigger purpose. The total surface of RPC will be close to 3400 m^2. The time resolution stays below 2 ns for rates up to 6 kHz/cm^2 and the efficiency is greater than 90% up to 5 kHz/cm^2 and is about 98% for 1 kHz/cm^2 [4, page 109].

1.4 Contribution of the Warsaw Group to CMS experiment - RPC Muon Trigger

1.4.1 Basic ideas

During LHC operation at its highest luminosity of 10^{34}cm^{-2}s^{-1}, 20 inelastic events will, on average, occur in every bunch crossing. Input rate will be of the order of 10^9 Hz, which should be reduced at least by a factor of 10^7 at the data acquisition level. In CMS, the trigger was divided into two steps. Level–1 trigger (FLT) operates on the data from each bunch crossing and have to limit the rate to 100 kHz. Then Level–2 trigger (SLT) operates on this subset of data and reduces it to 100 Hz. The system will be deadtimeless and the decision to skip or to collect the event at the FLT should be made in 128 bunch crossings. The FLT will contain muon and calorimeter FLT's, which will be combined together by a Global FLT. The Muon FLT will be actually based on three systems – one based on the RPC, the second on the DT and the third on CSC. Since the rates at 14 TeV are known with large uncertainties, the maximum FLT trigger rate must be lower than 100 kHz - 30 kHz seems a reasonable and safe value. It is equally divided between calorimeter and muon triggers.

1.4.2 The RPC based muon trigger

The RPC trigger must fulfill several major tasks

- measure transverse momentum of a muon,
- determine bunch crossing from which the muon comes,
- give the possibility to adjust the p_t threshold from a few GeV to 100 GeV.

Because of the time constraint, the algorithm has to be relatively simple. As can be seen on Fig. 1, 2 and 3 muon system comprises 4 detector layers called stations (marked

[13] Barrel region is divided into five wheels of twelve 30° sector each.

[14] Six layers with cathode strips oriented radially to measure azimuthal coordinate.

[15] One layer in each of MF1–MF4 and MS3–MS4 and two layers in each MS1-MS2 so sometimes it is called MS1, MS2′, MS2, MS2′.

orange). Muon is supposed to score hits in them and from the curvature of the track we want to deduce muon's transverse momentum. This will be based on our knowledge about the difference between the numbers of fired strips in each station. The idea of the algorithm is presented on Fig. 4. Station no. 2 was chosen as reference one. The p_t reconstruction is based on three numbers – $\Delta^{1,2}$, $\Delta^{2,3}$, $\Delta^{2,4}$. We call a group of such three differences – a pattern.

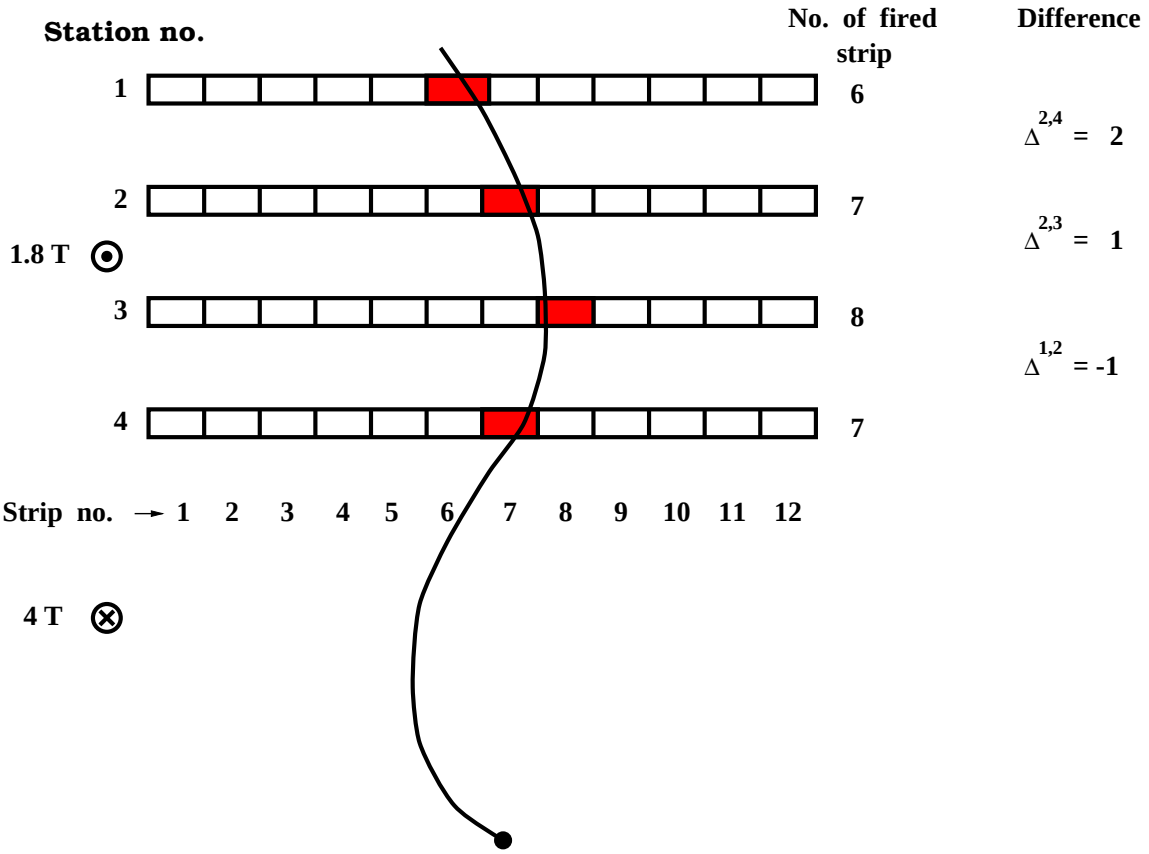

Figure 4: Example of four hit pattern

It seems easy and very accurate – one pattern corresponds to one range in p_t. But due to statistical fluctuations in multiple scattering and energy loss there is more than one pattern for each p_t. A set of hit patterns corresponds, therefore, to given p_t interval. Another difficulty is that the same pattern corresponds to different p_t muons in different η regions[16]. To tell a little bit more about algorithm, segmentation of the trigger should be discussed. In ϕ there are 1152 strips combined into 144 groups of 8. The groups of 8 are called segments and comprise 2.5 degree. Division in η is presented on the Fig. 5. The whole η region is divided into 39 projective towers. We group sectors from 4 stations in this same η tower.

From almost 2×10^5 RPC channels we finish with 5616 units called segments ($\Delta\phi = 2.5^\circ$ and $\Delta\eta \simeq 0.12$). Segments are the basic logical units for the RPC muon FLT. Each segment is based on 8 strips in the reference station (MS2). In the other stations more

[16] Magnetic field is not uniform in the whole detector.

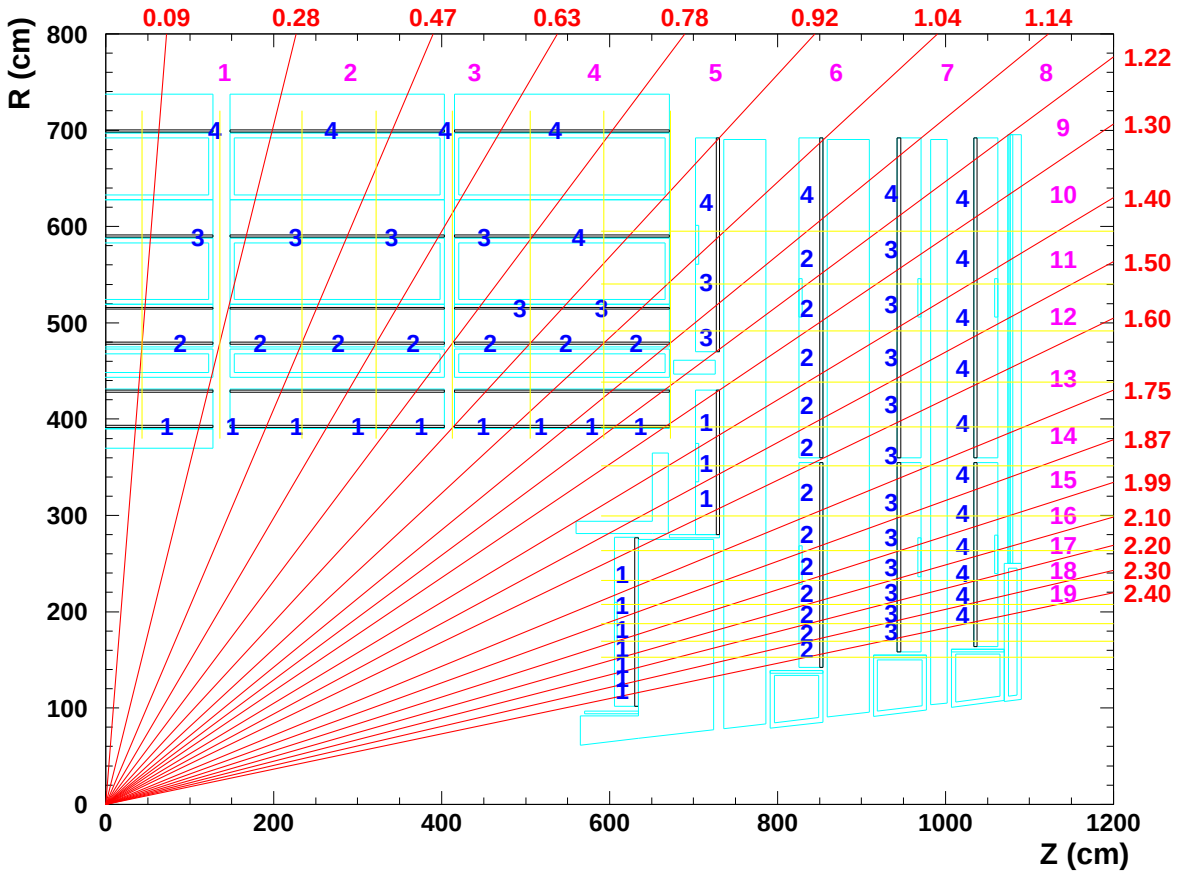

Figure 5: Division of the RPC trigger in η. Pink numbers denote towers, blue numbers refer to RPC layers.

strips are connected to a given segment to account for track bending. We shall call such region in space, subtended by all strips connected to a given segment – a cone. For each segment, a dedicated ASIC processor called PAC will perform pattern recognition, p_t evaluation and bunch crossing assignment. The prototype chip is being now designed in Warsaw[17]. It will be loaded with a set of predefined patterns[18] taken from the simulation. To each of them, definite momentum will be associated. The envisaged p_t binning is presented in Table 2.

No. of p_t bin	Range in p_t [GeV]	No. of p_t bin	Range in p_t [GeV]
1	1.0-1.2	13	10.0-12.0
2	1.2-1.5	14	12.0-14.0
3	1.5-2.0	15	14.0-17.0
4	2.0-2.5	16	17.0-20.0
5	2.5-3.0	17	20.0-25.0
6	3.0-3.5	18	25.0-30.0
7	3.5-4.0	19	30.0-35.0
8	4.0-5.0	20	35.0-40.0
9	5.0-6.0	21	40.0-50.0
10	6.0-7.0	22	50.0-70.0
11	7.0-8.0	23	70.0-100.0
12	8.0-10.0	24	> 100.0

Table 2: Binning in p_t

It has to be mentioned that due to the holes in geometrical acceptance[19] we accept a muon track candidate if at least 3 out of 4 stations were fired [7]. In this case all strips in the missing station are assumed to be hit. Another reason is that the efficiency of the RPC (see section 1.3.5) is less than 100%. In terminology used in the muon trigger group, tracks reconstructed on the base of hits in 4 stations are assigned quality bit 1 (also called 4/4), while these with only 3 have quality bit 0 (called 3/4). 4/4 muon always precedes 3/4 one.

Another important problem is reconstruction of muons with small p_t (i.e. up to 5-6 GeV). For triggering on such soft muons in the barrel, additional RPC stations MS1′ and MS2′ were designed[20]. In this case fluctuations in strip differences are so strong and

[17] In Warsaw University and Warsaw University of Technology.

[18] Pattern consists of 4 numbers corresponding to fired strips – we can also speak about it in terms of strip's differences. Chip will be designed in such a way that there will be a possibility to load another set of patterns during experiment's operation.

[19] The worst is the region between barrel and endcaps.

[20] Soft muons cannot reach outer most stations MS3 and MS4 due to energy losses in the calorimeters and the yoke [8].

number of valid patterns grows so rapidly that algorithms of grouping strips in 2,4 or even 8 are considered. This decreases the number of patterns and has little effect on the resolution.

After muon recognition and its p_t reconstruction segments from the same η tower are formed into so called ring[21]. The ring processor will choose 4 μ highest p_t in every ring. The next step is shifting this data to global trigger, where the four highest p_t muons in whole CMS are found. More informations about Muon Trigger in CMS experiment can be found in [9, 10].

1.5 Description of algorithm

During the studies of the 2μ trigger rates, RPC Muon Trigger Software – *MRPC* package – implemented in CMSIM 101 with geometry version no. 14 was used. The summary of its operation idea can be found in [12]. Only the most general steps are listed. They are labelled with corresponding routine names

- MRMARKTOWERS – performs assignment of hits to towers. It should be stressed that one hit may belong up to 3 towers.
- MRFINDTOWERS – finds towers in which hits are stored in at least 3 logical planes.
- MRCHECKCONES – performs the loop over hit towers and sectors calculating differences between strip numbers. Then compares found combinations with predefined patterns. If there is/are corresponding pair(s) it fills special table with reconstructed muons.
- MRSORTMUONS – muons are sorted according to p_t and quality bit. So called ghost muons are also suppressed.

The last function of routine MRSORTMUONS is of the crucial importance. It may happen that one μ "answers" in few detector segments. It is the inner feature of the algorithm because cones corresponding to different segments in reference station no. 2 may cover partially these same regions in other stations. It may happen that one pattern called "4 out of 4" is found in a given segment, and one (or more) "3 out of 4" in the neighbouring segment(s). There can also appear few patterns "3 out of 4" when μ missed one of the stations[22], or it did not respond due to its 2% inefficiency. Of course better algorithm, assuming knowledge about hit strips in whole detector, may be devised, but it can not be implemented in CMS hardware due to time limitations. The first turn was vetoing the nearest neighbours for selected μ – ghost suppression. On Fig. 6 "+" denotes picked up μ , "–" rejected candidates and "0" vetoed segments.

The muon selection is done according to the rules:

[21] 360° coverage in ϕ and $\simeq 0.12$ in η.

[22] Geometrical gaps.

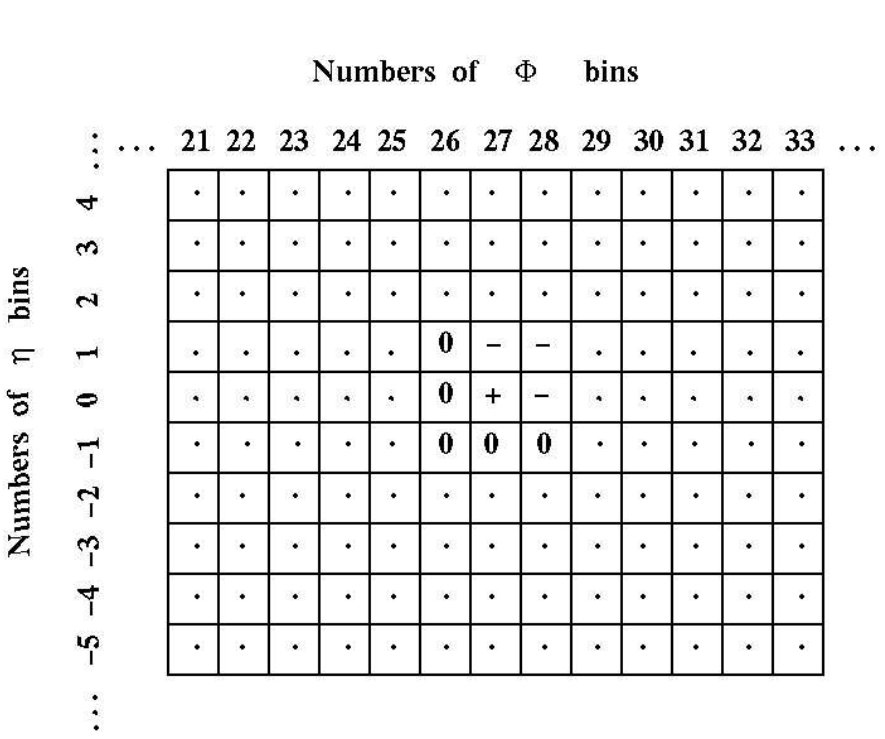

Figure 6: Example of veto algorithm in action

1. μ with higher quality bit is taken,

2. For muons with the same quality bit, one with the highest p_t is saved.

Of course apart from useful function – killing ghosts – it may cause rejection of the events in which two μ were pointing in the neighbouring segments. This will be examined in section 5.5. Analysing the trigger response to the simulated 2 μ events we found that existing algorithm is not sufficient. There were more events in which one μ from the pair was reconstructed as two[23], and the second one was not visible at all, than events with both generated μ properly reconstructed. For the purpose of this job it seemed more sensible to process muons one by one, to remain maximally independent from algorithm imperfections. Ratios between the real and the ghost rates will be presented in section 5.4. Still opened problems are:

1. Vetoing scenario to maximally cut off ghost events, without serious reduction of real events.

2. Making connections between segments in every ring.

3. Reduction of regions in which procedure of grouping strips for soft μ is applied.

[23] After veto procedure.

1.6 Aims of this thesis

Chosen subject of the M.Sc. thesis is closely connected with tasks for which Warsaw CMS Group is responsible. The main goals are listed below

- To calculate the double μ rates explicitly - not only in approximative way on the basis of single μ rates.
- To examine the main sources of the rate.
- To check out if the muon trigger segmentation and the spatial arrangement of its detectors suits scientific tasks which are planned to complete during the experimental run. This means searching the double μ events topology whether both muons coming from the same event, can be properly recognised and how large fraction of the rate will be rejected.
- To examine possibility of bad triggers:
  1. Due to superimposing of the single μ events coming from the different p-p collisions in this same bunch crossing.
  2. Due to the mentioned ghost production by envisaged reconstruction algorithm.
- To propose some improvements to the algorithm which can help in getting rid of ghosts. Consider the "price" to pay for these changes – increased rate rejection.

Rate estimates are important to know how high p_t^{cut} will be needed to stay below 15 kHz allocated to the whole muon trigger. The knowledge about contribution of different background processes to the rate and their topology may be helpful in preparing cuts extracting interesting events e.g. Higgs ones. Rate results are discussed in section 3.3 and 5.2. The influence of detector circumstances on correlation in pairs may be derived on the base of sections 4 and 5.5. The studies of the bad triggers are necessary to be aware of the purity of our signal. The knowledge about probability of bad event reconstruction will be crucial in the error estimation. If enlarging veto area is possible, it will have the influence on the number and logic of processors making muon selection.

2 Generation of 2 μ events

2.1 PYTHIA 5.7 a tool used in simulation.

As usually in this kind of job – simulation of the detector response for physical events – is divided into two steps. In the first one, a sample of specific events is generated by a Monte Carlo program. For this studies PYTHIA 5.7, written by Torbjörn Sjöstrand, was chosen [5]. In the second step this sample was processed by CMSIM – Monte Carlo program based on GEANT. Full detector geometry and algorithm of the RPC trigger was implemented in it.

Pythia 5.7 gives one a possibility to investigate hard or soft interactions in collisions of leptons, hadrons and photons. It is especially convenient for e^+e^-, ep and pp – typical particles used nowadays in high–energy physics machines. The heart of the event is generation of the hard process – in which two partons collide. Around this process initial and final state radiation is added – QED or/and QCD depending on electric and colour charge of interacting partons. Due to complication in calculations of the phase space program is optimised for 2→1 and 2→2 processes. Higher ones are generated on the base of these by sequence of branchings e.g. – $q \to qg$, $e \to e\gamma$. These branchings lead to cascades of partons, both in the initial and final state.

In the next step, coloured partons are transformed into colourless hadrons. Because this process is not yet well understood, several models exist – string fragmentation (SF), independent fragmentation (IF) and cluster fragmentation (CF). In Pythia the default one is string fragmentation, though there is a possibility to switch to the independent fragmentation scheme. Probabilistic nature of branchings processes

$$\text{jet} \to \text{hadron} + \text{remainder-jet}, \qquad \text{string} \to \text{hadron} + \text{remainder-string etc.}$$

underlies these models.

The last part of the event generation consists of the particle decays into stable or almost stable ones. Though it does not seem so difficult from the theoretical point of view as the fragmentation, it is not too simple. One reason is incomplete knowledge of decay properties of all particles – precise measurement of branching ratios is crucial there.

Pythia 5.7 gives possibilities of probing many physics reactions. Most important of them are listed below

- hard QCD processes – qg,gg → qq and similar
- soft QCD processes – diffractive and elastic scattering
- heavy quark production – top production in process $gg \to t\bar{t}$
- prompt photon production – qg → qγ
- deep inelastic scattering – ql → ql

- W/Z production
- Standard and non standard model Higgs production[24]
- gauge bosons scattering – WW$\rightarrow$ WW
- Production of new gauge bosons – Z′, W′
- production of fourth–generation fermions
- production of leptoquarks

Of course only the most important graphs have been included and in many cases only the approximation of the matrix elements is used. Unfortunately, the latest program version has no production and decays of supersymmetric particles implemented in it. Complete description of Pythia 5.7 can be found in [5].

Types of generated physics processes were listed in Appendix A, whereas tricks used to obtain sufficient statistic were described in Appendix B.

2.2 Reliability of the results

Studies of the agreement between the results given by Pythia and obtained from the experiments are presented in technical note [11]. The main conclusions are

- For the highest possible energy in p$\overline{p}$ collisions in Tevatron the agreement for $b \rightarrow \mu$ was within one σ for high p_t^{cut} ($p_t^{cut} > 25$ GeV). Going down with p_t^{cut} the difference become larger – few standard deviations. Experimental results were about two times greater than simulation.
- For different structure functions CTEQ2L from Pythia 5.7 and EHLQ from Pythia 5.6 the muon rates are similar for low p_t^{cut} (around few GeV), whereas increasing the cut the difference approaches the factor five – older Pythia version produces higher results.

Thus the results presented in this simulation for $\sqrt{s} = 14$ TeV are expected to agree with the future experimental results within a factor of two to five. The agreement will be probably better for high cuts.

2.3 Terminology

To ensure the maximal transparency in analysing results of simulations, some criteria of classification have been applied. Events were arranged according to the priority of a muon source. The priority of sources is shown below in descending order

- particles containing *top* quark

[24] Within the framework of two-doublets scenario – two charged states $H^{\pm}$ and three neutral h, H, A.

- Z^0, W bosons and virtual γ from a Drell-Yann process
- J/Ψ – $(\psi(1S))$ particle
- particles containing *beauty* quark
- particles containing *charm* quark other than J/ψ
- kaons – $K^{\pm}$
- pions – $\pi^{\pm}$
- other particles containing s, d, u quarks

J/ψ particle was treated in special way because it can directly decay into 2 μ[25]. It should be stressed that cascade decays were taken into account and the event was classified according to the μ ancestor with the highest priority. Names "2 μ from *source_name* events" and "2 μ from *source_name*" are commonly used. First means that one – μ_1 comes from the decay of particles belonging to category "*source_name*" and the second – μ_2 from the source with lower or at most equal priority. Second type of name is used if both μ comes from this same type of source. Below few examples are given to explain it

- $Z^0 \to \mu^-\mu^+$ – belongs to category "2 μ from Z^0" and of course to "2 μ from Z^0 events"
- $Z^0 \to \mu_1$, $K^{\pm} \to \mu_2$ – belongs to category "2 μ from Z^0 events"[26]
- $B^- \to \overline{D} \to \mu_1$, $\pi^{\pm} \to \mu_2$ – belongs to category "2 μ from beauty events"
- $B^- \to J/\psi \to \mu_1$, $\pi^{\pm} \to \mu_2$ – belongs to category "2 μ from J/ψ events"
- $B^- \to J/\psi \to \mu_1\mu_2$ – belongs to category "2 μ from J/ψ"

On account of special interest connected with μ from *beauty* and *charm* decays, additional categories were introduced

- "2 μ from *beauty* grandparents"
- "2 μ from *beauty* parents"
- "2 μ from *charm* grandparents"
- "2 μ from *charm* parents"

[25] Problem of identification both of them will be examined in sections 4 and 5.5.

[26] One μ from Z^0 may simply point into the region not covered by the muon detector.

Words *parents* and *grandparents* denote on which level in the decay tree beauty or charm particle appeared. Division into categories with suffix "events" and without it is conserved. It assures more detailed analysis for these important channels. Additionally in minimum bias division into two classes – so called "correlated" and "uncorrelated" events – was introduced. The event belongs to the first of them when both μ had in the decay tree ancestor with beauty or charm quarks. Otherwise it is classified as uncorrelated event. Category "2μ from uds events" means that both μ came from particle built only from the combination of 3 lightest quarks, but not from π or K.

3 Two muon rates on the generation level

3.1 Acceptance

In this section so called accepted events are discussed. The acceptance was defined as a probability of a muon reaching at least 2 out of 4 high p_t stations (disregarding MS1′ and MS2′). We can think about it as geometrical acceptance, latter in this thesis we introduce trigger acceptance, which means that μ was recognised and p_t assignment was done. These functions are performed on the base of hits in at least 3 logical stations in the same cone. Thus trigger needs more conditions to be fulfilled than the geometrical acceptance. Comparing accepted rates with trigger ones we are given the information about the efficiency of events recognition. We can also learn to know the quality of p_t reconstruction – how large is the shift towards higher p_t values.

Acceptance varies with p_t and η of a muon. Separate results for μ^+ and μ^- are given on Fig. 7 and 8. The transverse momentum axis was labelled with "p_t bin" which denotes that bins are numbered with p_t codes – to get the corresponding value in GeV use Table 2 on page 13. The η axis was numbered with η towers numbers – corresponding values in the pseudorapidity units can be obtained from Fig. 5 on page 12.

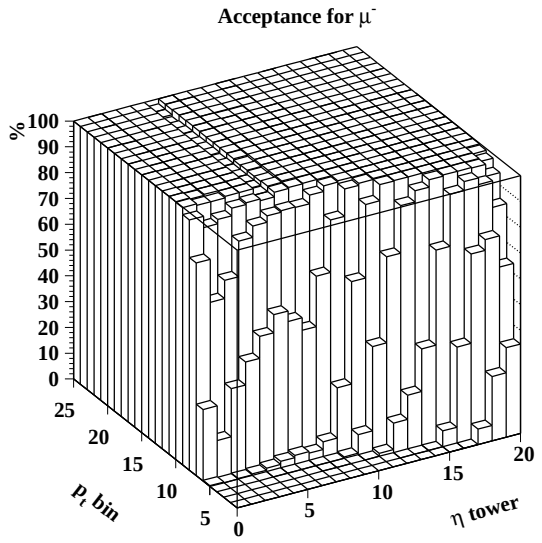

Figure 7: Acceptance for μ^-

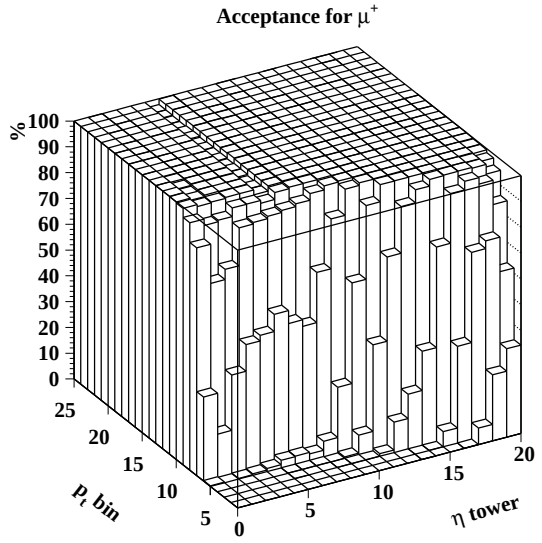

Figure 8: Acceptance for μ^+

These results come from the CMSIM simulation of a μ behaviour in CMS detector. Muons were produced in vertex. For very soft μ – with $p_t \leq 2.5$ GeV – acceptance is different from zero only in a high η region. It reaches 34% for p_t bin [1.0,1.2] GeV in the last η station[27]. It shifts towards lower η with the increase of p_t. Above 4 GeV, the p_t acceptance reaches at least 97%. In most of the remaining area it is almost equal to 100%. But there is one η region – from 0.78 to 0.92 (tower 5) – where it decreases to only 97–98%. It is the region of gaps between barrel and forward areas – see Fig. 5.

[27] There is very thick absorber – almost 2m HCAL.

Comparison of μ^+ and μ^- figures reveals some differences (sometimes on the level of even 5–6%) for low p_t in the barrel region. The reason of asymmetries lies in staggering of muon stations shown on Fig. 2 in section 1.3. Asymmetric arrangement is necessary to assure high acceptance. More informations about asymmetries can be found in [8].

3.2 Accepted 2 μ events

Large data sample were simulated. Statistical information are collected in the Table 3. Total cross sections, necessary for rate calculations, are also given.

Simulation Type	Number of generated events	σ_{tot} [mb]
Minimum bias	619×10^6	5.523×10^1
J/ψ production	11.7×10^6	1.694×10^{-1}
W production	2.21×10^6	4.416×10^{-4}
Z^0 production	262×10^3	1.395×10^{-4}
top production	579×10^3	6.084×10^{-7}
Drell-Yan	900×10^3	9.765×10^{-4}

Table 3: Statistics of different types of generate events

Numbers of accepted 2 μ events, are given in Table 4.

The term "large volume" denotes that these numbers are for the whole data collection region – including not only tracker but also calorimeters. This enlargement was introduced to avoid event rejection due to curlying in magnetic field. No procedures simulating behaviour of muons or its charged parents[28] in magnetic field and detector material were applied at this stage.

For the decay volume equal to the tracker's – this case coresponds to the term "small volume" – some events were rejected. Apart from decay volume decrease, some checks on the influence of magnetic field were done. For charged particles – $K^{\pm}$, $\pi^{\pm}$, a new decay vertex was simulated. Muon momentum vector was assumed to preserve its absolute value[29], but it was apropriately rotated. The rotation was made in such a way, that the relative orientation, in the $r - \phi$ plane, of hadron's and muon's momentum vectors was preserved.

Numbers of accepted events in both cases are accumulated in Table 4. Large decrease in events number for minimum bias is explained on Figs. 9 – 12, which are transverse momentum distributions[30] for muons with lower and higher p_t satisfying geometrical cuts

[28] Mainly $K^{\pm}$ and $\pi^{\pm}$.

[29] Energy loses and multiple scattering for hadrons not included.

[30] The bin width of these distributions are defined in $log\, p_t$. Thus the shapes of these curves are valid, whereas the ratios between them are not correct.

Simulation type	μ source	$N_{acc\ large}$	$\sigma_{acc\ large}$ [mb]	$N_{acc\ small}$	$\sigma_{acc\ small}$ [mb]
Minbias	2μ from anything	27352	2.440×10^{-3}	12829	1.145×10^{-3}
Minbias	2μ from π,K events	15167	1.353×10^{-3}	4305	3.841×10^{-4}
Minbias	2μ from K events	9271	8.271×10^{-4}	2640	2.355×10^{-4}
Minbias	2μ from K	2506	2.236×10^{-4}	731	6.522×10^{-5}
Minbias	2μ from π events	5896	5.260×10^{-4}	1665	1.485×10^{-4}
Minbias	2μ from π	5861	5.229×10^{-4}	1655	1.477×10^{-4}
Minbias	2μ from b,c events	11503	1.026×10^{-3}	7829	6.985×10^{-4}
Minbias	2μ from c events	4583	4.089×10^{-4}	2377	2.121×10^{-4}
Minbias	2μ from c	2677	2.388×10^{-4}	1542	1.376×10^{-4}
Minbias	2μ from c grandparent events	3859	3.443×10^{-4}	2178	1.943×10^{-4}
Minbias	2μ from c grandparents	1256	1.121×10^{-4}	912	8.137×10^{-5}
Minbias	2μ from c parent events	3460	3.086×10^{-4}	2068	1.845×10^{-4}
Minbias	2μ from c parents	619	5.523×10^{-5}	579	5.166×10^{-5}
Minbias	2μ from b events	6920	6.174×10^{-4}	5452	4.864×10^{-4}
Minbias	2μ from b	5340	4.764×10^{-4}	4595	4.100×10^{-4}
Minbias	2μ from b grandparent events	6171	5.506×10^{-4}	5100	4.550×10^{-4}
Minbias	2μ from b grandparents	2504	2.234×10^{-4}	2478	2.211×10^{-4}
Minbias	2μ from b parent events	5695	5.081×10^{-4}	4788	4.272×10^{-4}
Minbias	2μ from b parents	1746	1.558×10^{-4}	1754	1.565×10^{-4}
Minbias	2μ from "uds" particles	347	3.096×10^{-5}	347	3.096×10^{-5}
Minbias	2μ from J/Ψ events(b decays)	339	3.025×10^{-5}	350	3.123×10^{-5}
Minbias	2μ from J/Ψ (b decays)	284	2.534×10^{-5}	299	2.668×10^{-5}
Minbias	2μ from J/Ψ parent events(b decays)	335	2.989×10^{-5}	348	3.105×10^{-5}
Minbias	2μ from J/Ψ parent(b decays)	284	2.534×10^{-5}	299	2.668×10^{-5}
J/Ψ production	2μ from J/Ψ events	1537	2.224×10^{-5}	1500	2.171×10^{-5}
J/Ψ production	2μ from J/Ψ	1489	2.155×10^{-5}	1482	2.145×10^{-5}
J/Ψ production	2μ from J/Ψ parent events	1537	2.224×10^{-5}	1500	2.171×10^{-5}
J/Ψ production	2μ from J/Ψ parent	1489	2.155×10^{-5}	1482	2.145×10^{-5}
W production	2μ from W events	5134	1.026×10^{-6}	2863	5.721×10^{-7}
W production	2μ from W	1206	2.410×10^{-7}	523	1.045×10^{-7}
Drell-Yan	2μ from γ events	2518	2.732×10^{-6}	2487	2.698×10^{-6}
Drell-Yan	2μ from γ	2508	2.721×10^{-6}	2479	2.690×10^{-6}
Z^0 production	2μ from Z^0 events	5091	2.711×10^{-6}	4767	2.538×10^{-6}
Z^0 production	2μ from Z^0	4696	2.500×10^{-6}	4541	2.418×10^{-6}
t production	2μ from t events	78795	8.280×10^{-8}	65666	6.900×10^{-8}
t production	2μ from t	51829	5.446×10^{-8}	44506	4.677×10^{-8}

Table 4: Numbers of accepted events in "large" and "small" volumes

– $p_t \geq 1$ GeV and $|\eta| \leq 2.4$ – Figs. 9 and 10, and these which have already been accepted – Figs. 11 and 12.

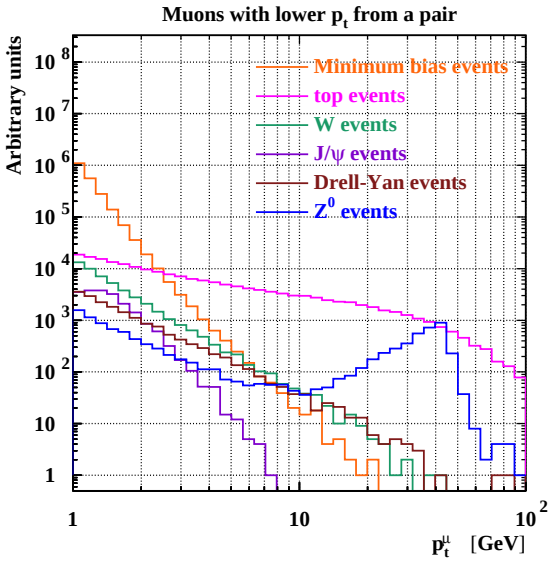

Figure 9: Transverse momentum distribution. Geometrical cuts only.

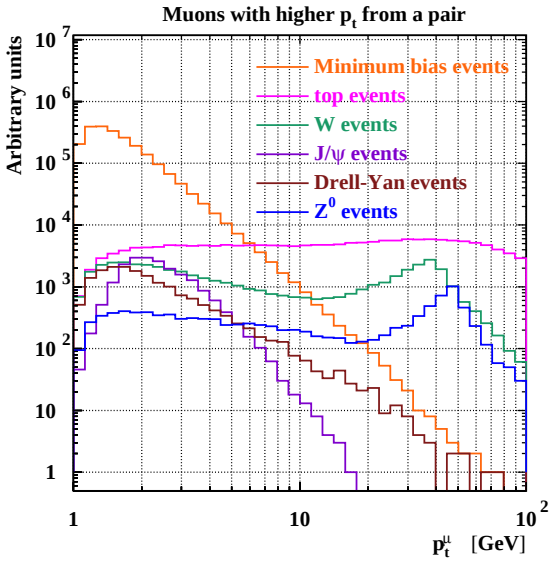

Figure 10: Transverse momentum distribution. Geometrical cuts only.

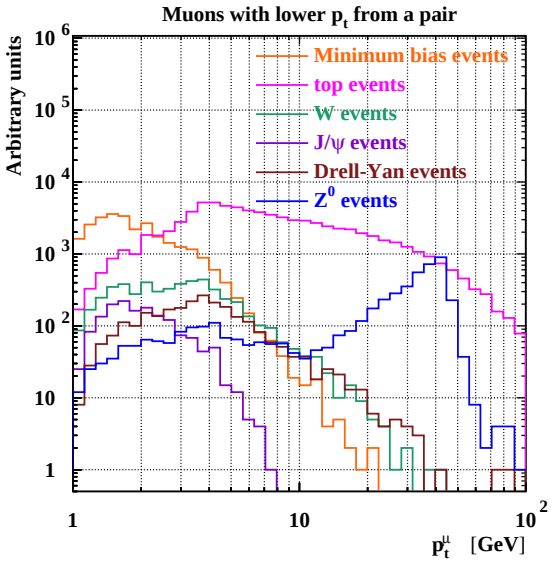

Figure 11: Transverse momentum distribution with acceptance applied.

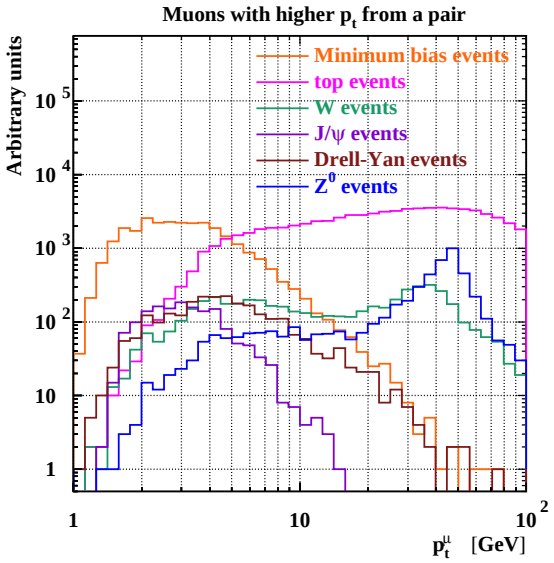

Figure 12: Transverse momentum distribution with acceptance applied.

For minimum bias events and J/ψ events the p_t distributions are soft. Large differences between distributions for lower and higher p_t muons for W and top come because that lower p_t muon comes from kaon or pion decay. Z^0 spectrum has characteric Jacobian peak above 40 GeV. In Tables 5 and 6 the percentage of events after cuts and accepted events in the region of varying geometrical acceptance ($1.0 < p_t < 4$ GeV/c) are given for lower and higher p_t muons.

Simulation Type	% μ satisfying cuts – $p_t > 1$ GeV and $\|\eta\| < 2.4$	% μ accepted i.e. at leats 2 high p_t station reached
Minimum bias events	99.92	94.00
J/ψ events	99.56	94.34
W events	97.24	73.65
Z^0 events	59.67	13.12
top events	69.48	27.44
Drell-Yan events	94.02	59.45

Table 5: Percentage contribution in the p_t region of 1–4 GeV/c, for lower p_t muons

Simulation Type	% μ satisfying cuts – $p_t > 1$ GeV and $\|\eta\| < 2.4$	% μ accepted i.e. at leats 2 high p_t station reached
Minimum bias events	97.76	71.01
J/ψ events	91.83	72.93
W events	45.98	14.13
Z^0 events	35.37	3.22
top events	24.39	2.94
Drell-Yan events	88.40	41.26

Table 6: Percentage contribution in the p_t region of 1–4 GeV/c for higher p_t muons

Figs. 13 – 16 present differential cross sections in η for lower and higher p_t muons. Most of the minimum bias and J/ψ events are accepted in the forward direction. These plots allow one to check in the easy way if the lower p_t muon predominantly comes from heavy source, or if there is a strong contribution of K and π decays.

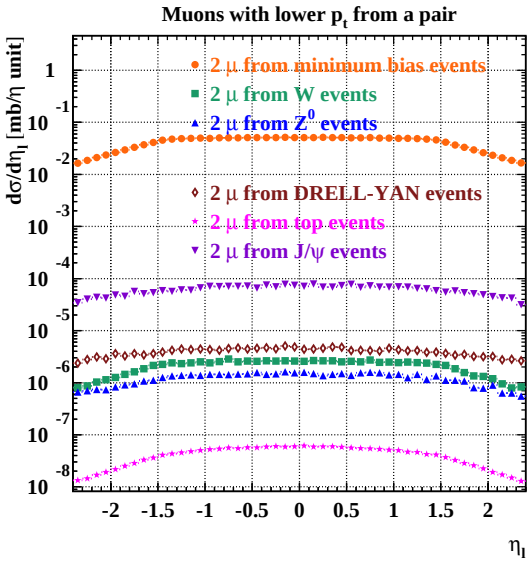

Figure 13: Distribution in η with only cuts applied – all simulations

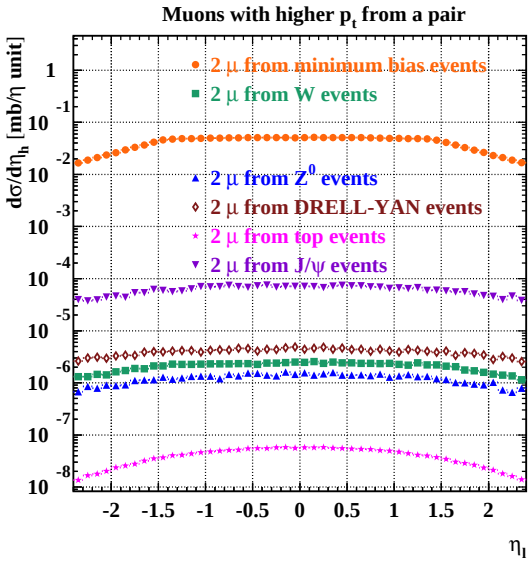

Figure 14: Distribution in η with only cuts applied – all simulations

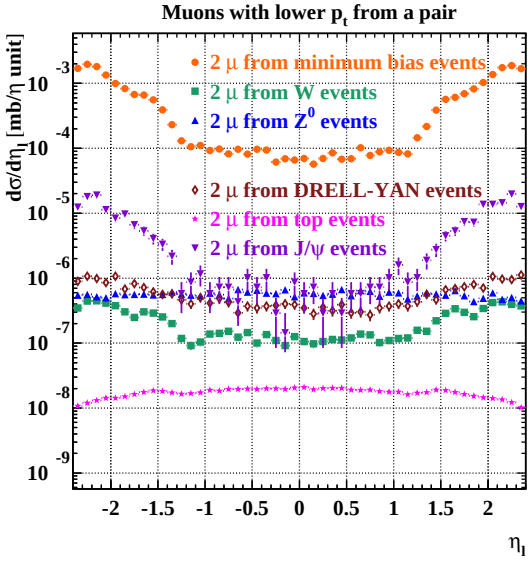

Figure 15: Distribution in η with acceptance applied – all simulations

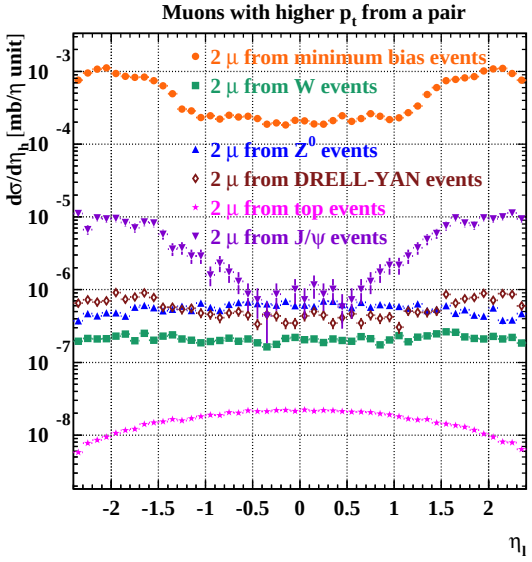

Figure 16: Distribution in η with acceptance applied – all simulations

3.3 The double μ rates

When one knows cross section on the interesting process – σ_{acc}, and luminosity of the machine usually denoted by L, there is very simple formula to count rate:

$$RATE = \sigma_{acc} \cdot L \tag{4}$$

The 2 μ rate integrated above $p_t = 1$ GeV can be read from the Table 4. Because luminosity of $10^{34}\mathrm{cm}^{-2}\mathrm{s}^{-1}$ can be expressed as $10^{7}\mathrm{mb}^{-1}\mathrm{s}^{-1}$, the numbers from Table 4 make it clear that total 2μ rate reaches the value of 12 kHz.

The rates in this report are integrated and based on p_t distribution curves for lower p_t muon in a pair. To obtain the rate for the specific p_t^{cut}, the integration of the differential p_t distribution curve from p_t^{cut} to ∞ (in principle 100 GeV is infinity) should be done:

$$RATE(p_t^{\mu_1} \geq p_t^{cut}, p_t^{\mu_2} \geq p_t^{cut}) = \frac{L \cdot \sigma_{total}}{N_{total}} \cdot \int_{p_t^{cut}}^{100GeV} F(p_t)\, dp_t \tag{5}$$

where L – luminosity of the machine, σ_{total} – total cross section, N_{total} – total number of simulated events, $F(p_t)$ denotes differential p_t distribution curve – $\frac{dN}{dp_t}$. Examples of $F(p_t) \cdot \Delta p_t$ distribution curves were given in section 3.2.

Behaviour of the integrated rate in the p_t range from 1GeV to 100 GeV is presented on the Fig. 17, where curves for all major types of events and the sum of them are plotted.

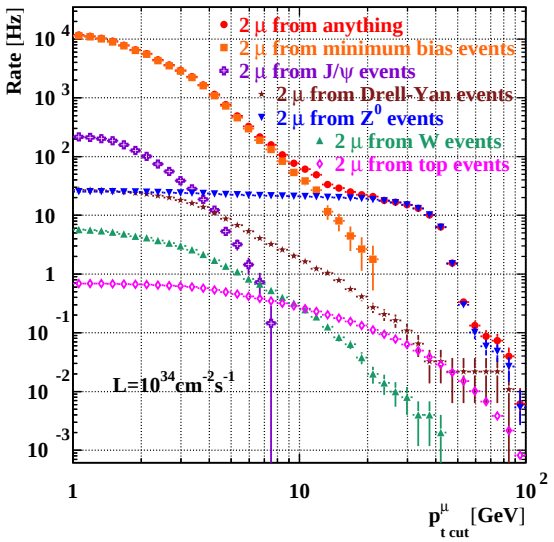

Figure 17: Integrated 2μ rate from all sources. Only acceptance was imposed. Case of "small volume".

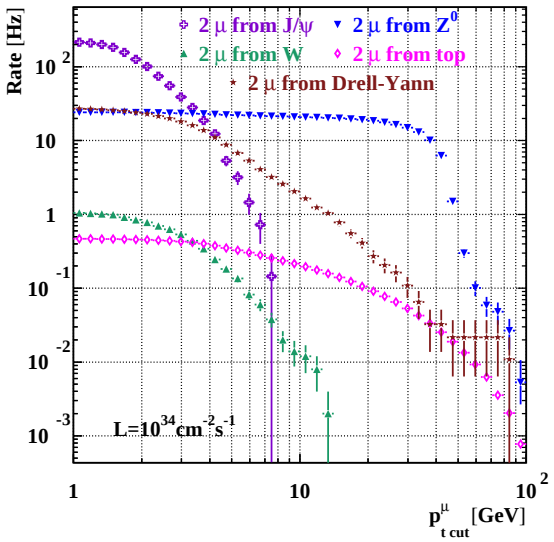

Figure 18: Integrated 2μ rates from "heavy" sources. Only acceptance was imposed. Case of "small volume".

From the first look it can be seen that total rate (full red dots) is practically dominated by two sources – minimum bias for p_t^{cut} up to about 10 GeV and some, Z^0 events above. The abrupt fall of the rate above 40 GeV is caused by a Jacobian p_t distribution for muons from Z^0. In very high p_t region the contribution of Drell–Yan and top events began play some part (about 10 % of the total). Other sources are negligible. It may be interesting to compare the rates other than minimum bias when more pure form of it is taken into account. It should be stressed that name "2μ from W event" means that only one μ

has W ancestor for sure. Both μ comes from W, when curve for this is named "2μ from W". Analogically in other cases. Comparison of Figs. 17 and 18 suggests that for muon sources which can exactly produce 2μ in the final state – i.e. J/ψ, Drell–Yan process, Z^0 – differences are almost unreadable. The confirmation of this fact can be found in the Table 4. In the case of top, and especially W, the drop in the rate is remarkable – about 5 times, because direct decay into pair of muons is impossible.

Figs. 19 – 24 were given to study minimum bias rate in details. Important is that 2μ rate from minimum bias is dominated by beauty and charm particle decays. Decays of the particles built of three lightest quarks have significant contribution only for the lowest p_t^{cut}. On account of introducing categories in which the source of both μ is very sharply defined – "2μ from b parents" and "2μ from c parents" – one can say that the rate from beauty particles, has advantage over charm in the whole investigated range of variables. It is worth emphasising that it does not depend on the assignment of source priority.

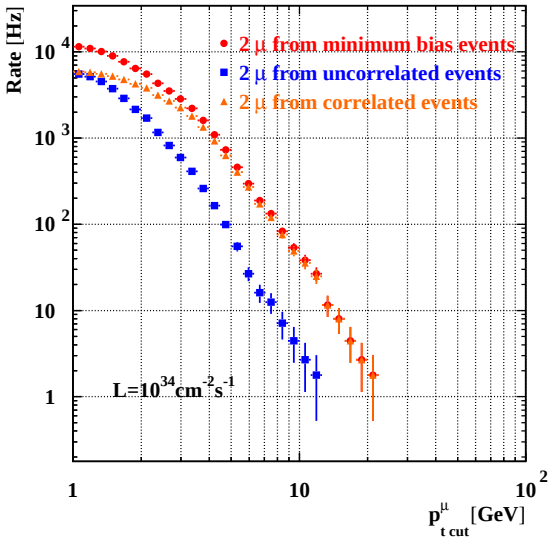

Figure 19: Integrated 2μ rates from different classes in minimum bias. Only acceptance was imposed. Case of "small volume".

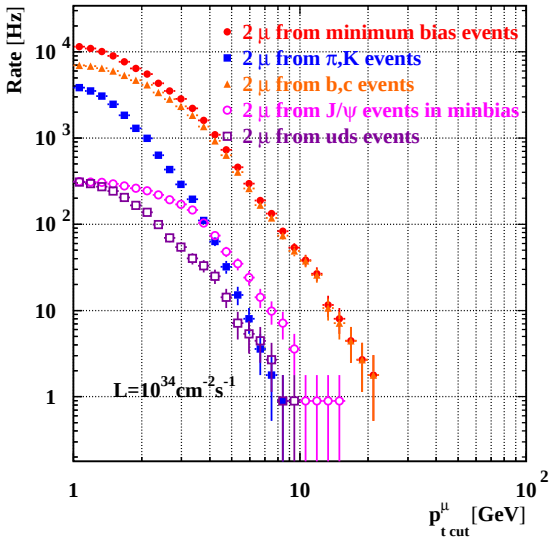

Figure 20: Integrated 2μ rates from different classes in minimum bias. Only acceptance was imposed. Case of "small volume".

3.4 Comparison of real and fake 2μ rates

Now lets spend some time on so called "fake 2μ rate". When we have more than one p-p collision in every bunch crossing there is some probability of faking of a real, double μ event by two single μ ones. If two single μ events appear in this same bunch crossing it will be probably impossible to distinguish them from a double μ event[31]. The knowledge of single μ rate is needed to find probability of the single μ event appearance in one p-p

[31]Some possibility may be given by trying to reconstruct vertex of origin because of about 7cm bunch length.

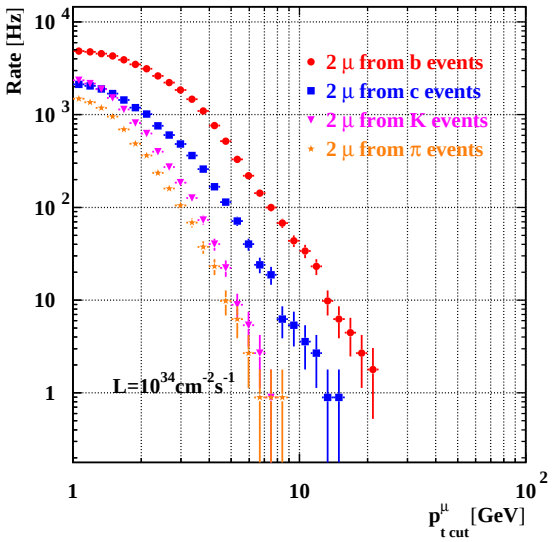

Figure 21: Integrated 2μ rates from different classes in minimum bias. Only acceptance was imposed. Case of "small volume".

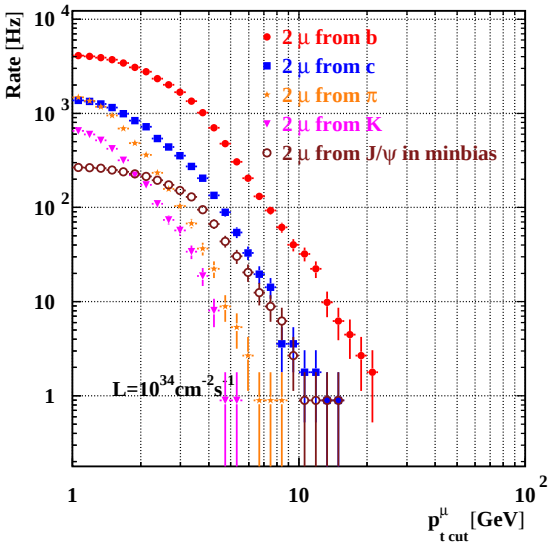

Figure 22: Integrated 2μ rates from different classes in minimum bias. Only acceptance was imposed. Case of "small volume".

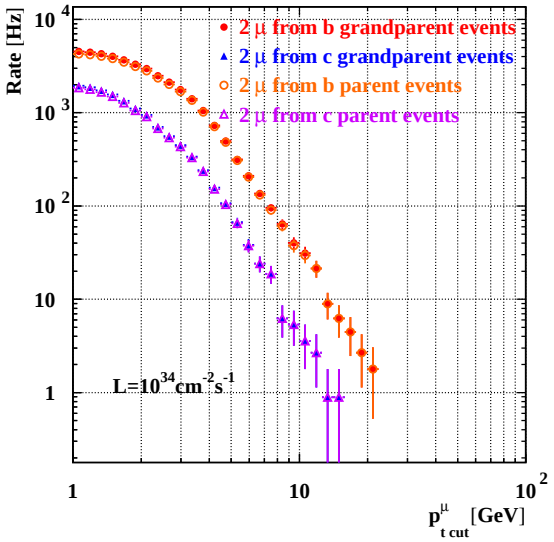

Figure 23: Integrated 2μ rates from different classes in minimum bias. Only acceptance was imposed. Case of "small volume".

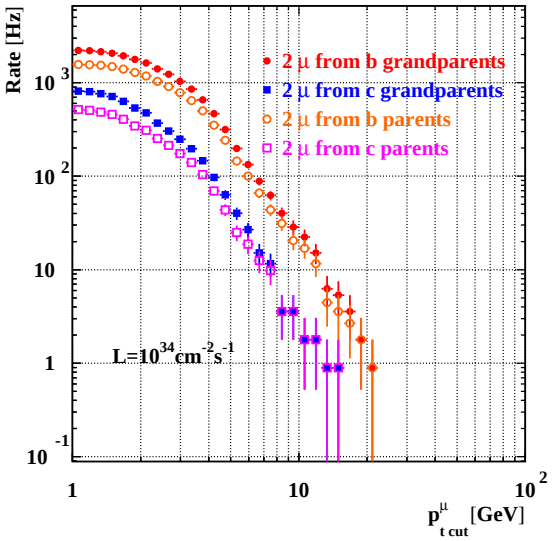

Figure 24: Integrated 2μ rates from different classes in minimum bias. Only acceptance was imposed. Case of "small volume".

collision. Some simulations of it were done earlier, the author has done his own, in which exactly the same conditions (volume and allowed particle decays) as for double μ rate were used. Figure 25 presents single μ rates on which calculations were based.

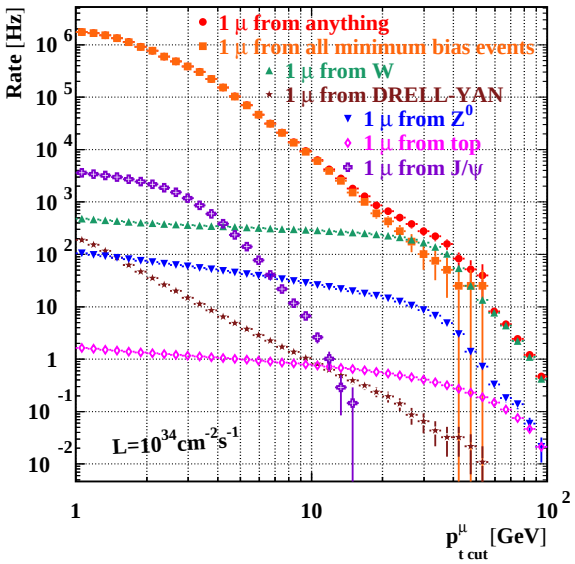

Figure 25: Single μ rate. Only acceptance applied. Case of "small volume".

The plot for luminosity $L = 10^{33}\text{cm}^{-2}\text{s}^{-1}$ can be obtain from this one by simple division by ten. Probability of a single μ event was calculated from the single μ rate according to formula:

$$p_{sin} = \frac{Rate_{sin}}{L \cdot \sigma_{tot}} \tag{6}$$

where p_{sin} denotes probability of appearance of single μ event, $Rate_{sin}$ – rate for this, L – luminosity and σ_{tot} – total inelastic cross section[32]. Exactly the same results for this probability will be obtained for $L = 10^{33}\text{cm}^{-2}\text{s}^{-1}$. Using this probabilities for different p_t cut, the fake double μ rate was calculated from the Formula (7) based on convolution of Poisson and binomial distributions:

$$Rate_{fake} = \sum_{N=2}^{\infty} P_\mu(N) \cdot B^N_{k\geq 2}(p_{sin}) \cdot f \tag{7}$$

where

- $P_\mu(N)$ – denotes probability of appearance of N p-p collisions which obeys the Poisson statistics with a mean μ which depends on the machine's luminosity. It is very good approximation – all conditions are fulfilled. The number of protons

[32] $\sigma_{tot} = 55.4$ mb coming from Pythia was taken.

in each bunch is very high – $\approx 10^{11}$, and the probability of interaction for defined particles very low.

- $B^N_{k\geq 2}(p_{sin})$ – probability of appearance of at least two single μ events among N p-p collisions. It is calculated from the binomial distribution with the probability of success p_{sin}. To avoid numerical problems the probability of zero and one success among N trials was calculated and then the sum of it was subtracted from unity:

$$B^N_{k\geq 2}(p_{sin}) = 1 - B^N_{k=0}(p_{sin}) - B^N_{k=1}(p_{sin}) \tag{8}$$

- f=40 MHz – number of bunch crossing per second. This value does not depend on luminosity[33].

The sum in the formula (7) could not be really performed to infinity. Cutting it at fourty for $\mu = 20$ and at twenty for $\mu = 2$ is precise enough.

On Figs. 26 – 29 comparison between real and fake rates and its sources for $L = 10^{34}\text{cm}^{-2}\text{s}^{-1}$ and $L = 10^{33}\text{cm}^{-2}\text{s}^{-1}$ was given. It was found sensible to cut plots at $2.5 \cdot 10^{-7}$ Hz, since the lowest value for the real rate is about 0.01 Hz.

Conclusions are as follows

- The fake rate for the highest luminosity exceeds real one by an order of magnitude for low p_t^{cut}.

- Fortunately the fake rate falls down quickly with a rise of p_t cut. At high p_t^{cut} it can be neglected.

- The fake rate in the region where it is important – low p_t – is caused by minimum bias events. For high p_t^{cut} the contribution of W begin to play a significant part. Other sources are marginal[34].

- The total fake rate is not the simple sum of the different fake rates. The reason is that to calculate total fake rate one does not simply sum fake rate curves for all examined sources, but sums all single μ rates curves to calculate probability – p_{sin} – and then follows procedure described by the equation (7).

- In the case of $L = 10^{33}\text{cm}^{-2}\text{s}^{-1}$ the fake rate is the simple rescaling of this for $L = 10^{34}\text{cm}^{-2}\text{s}^{-1}$. The rescaling factor is equal to one hundredths, which is the ratio of squared mean values of p-p collisions' multiplicities[35] in one bunch crossing for examined luminosities.

The main impression is that the fake rate does not cause serious danger even for the highest luminosity. Even for $p_t^{cut} > 4 - 5$ GeV – probably the lowest which will be introduced during experiment operation – the dominance of real rate over fake is achieved.

[33] Number of circulating bunches will be constant ≈ 3500.

[34] Top contribution is so small that there was no sense to present it.

[35] Equivalently the ratio of squared luminosities.

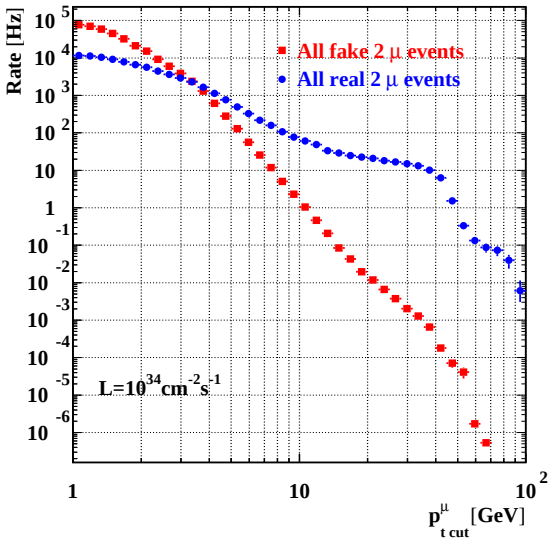

Figure 26: Comparison of the total real and fake 2μ rates. Only acceptance was imposed. Case of "small volume".

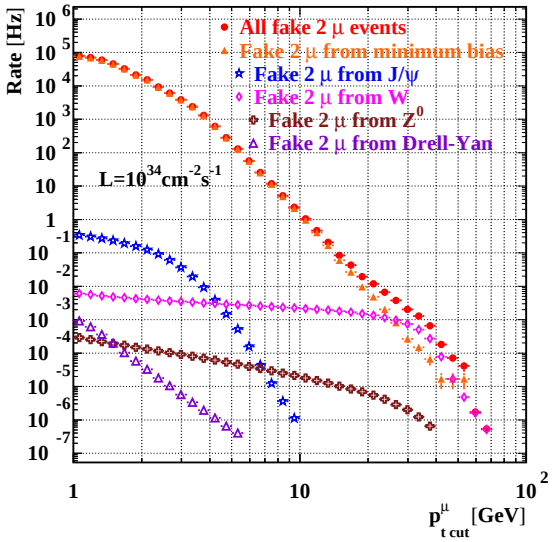

Figure 27: Different sources of the 2μ fake rate. Only acceptance was imposed. Case of "small volume".

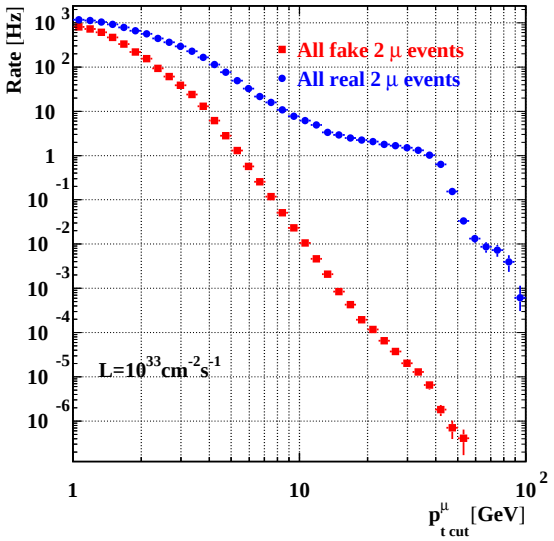

Figure 28: Comparison of the total real and fake 2μ rates. Only acceptance was imposed. Case of "small volume".

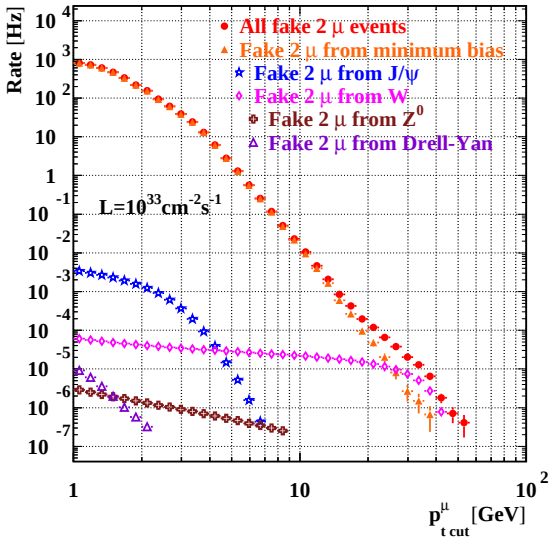

Figure 29: Different sources of the 2μ fake rate. Only acceptance was imposed. Case of "small volume".

4 Correlations in μ pairs on the generation level

In this section we discuss the spatial correlations between two muons in physical events (the only cut imposed is acceptance condition) – not disturbed by interaction with detector material and bending in magnetic field. These effects will be included in results presented in section 5.5. The realistic segmentation of the trigger in ϕ and η was applied (see section 1.5 for details).

The most important class of figures are these which present differences in η and ϕ between lower and higher p_t muons in a pair. Difference in η is always $\Delta\eta = |\eta_l - \eta_h|$. The difference in ϕ defined as follows:

$$\Delta\phi = \begin{cases} |\phi_h - \phi_l| & \text{for } |\phi_h - \phi_l| \leq 72 \\ 144 - |\phi_h - \phi_l| & \text{for } |\phi_h - \phi_l| > 72 \end{cases} \tag{9}$$

One should remember that these differences are calculated in terms of numbers of sectors and towers.

Trigger segmentation causes large fine granularity histograms. Number of histogram's fine bins is $39 \times 73 = 2847$ for scatter plots presenting $\Delta\eta$ and $\Delta\phi$. For the plot of ϕ_l vs ϕ_h it is even worse – we have 20736 bins. In some cases, when statistics of accepted events was extremely small fluctuations between neighbouring channels become significant. In spite of this at least qualitative conclusions can be derived in all cases. Most figures were done for $p_t^{cut} = 1$ GeV imposed on both muons – Figs. 30 – 60, and some for $p_t^{cut} = 1$ GeV – Fig. 61 – 68.

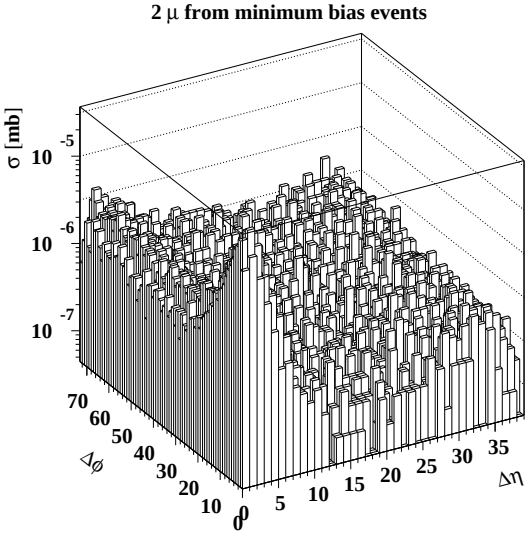

Figure 30: Dependence between $\Delta\eta$ and $\Delta\phi$ for minimum bias events in the case of $p_t^{cut} = 1$ GeV.

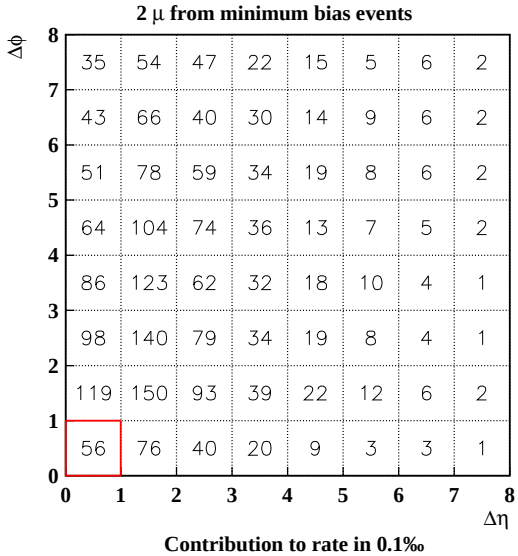

Figure 31: Contributions to the minimum bias rate from the region of small differences in η and ϕ for $p_t^{cut} = 1$ GeV.

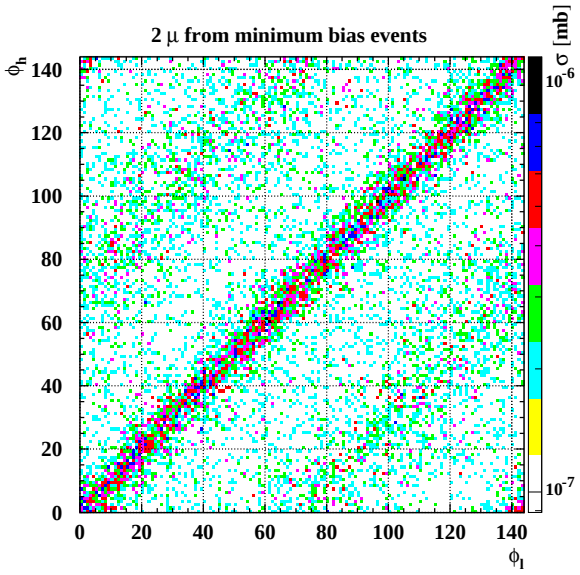

Figure 32: Dependence between ϕ of lower and higher p_t muons for minimum bias events in the case of $p_t^{cut} = 1$ GeV.

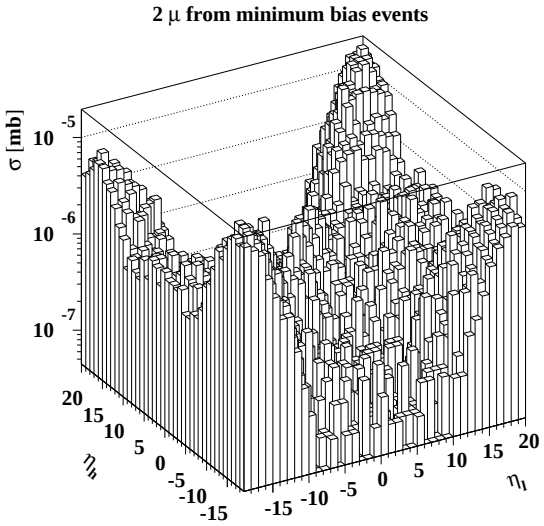

Figure 33: Dependence between η of lower and higher p_t muons for minimum bias events in the case of $p_t^{cut} = 1$ GeV.

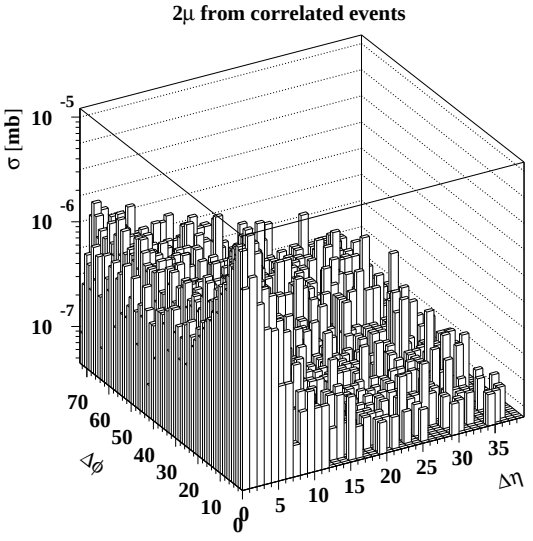

Figure 34: Dependence between $\Delta\eta$ and $\Delta\phi$ for correlated events in the case of $p_t^{cut} = 1$ GeV.

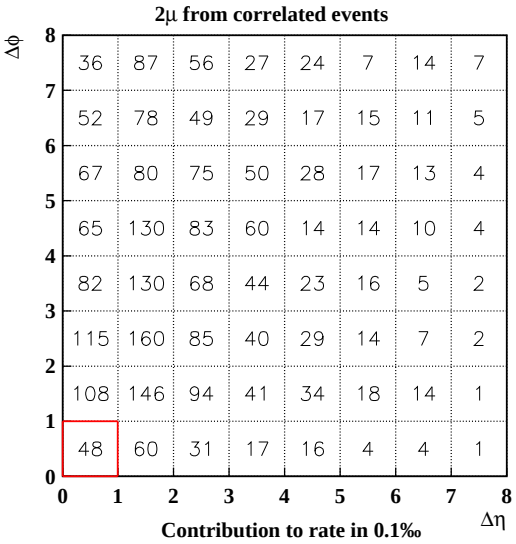

Figure 35: Contributions to the correlated rate from the region of small differences in η and ϕ for $p_t^{cut} = 1$ GeV.

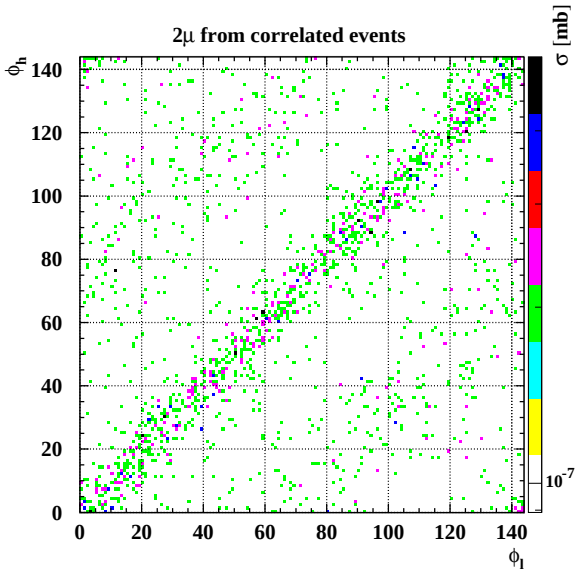

Figure 36: Dependence between ϕ of lower and higher p_t muons for correlated events in the case of $p_t^{cut} = 1$ GeV.

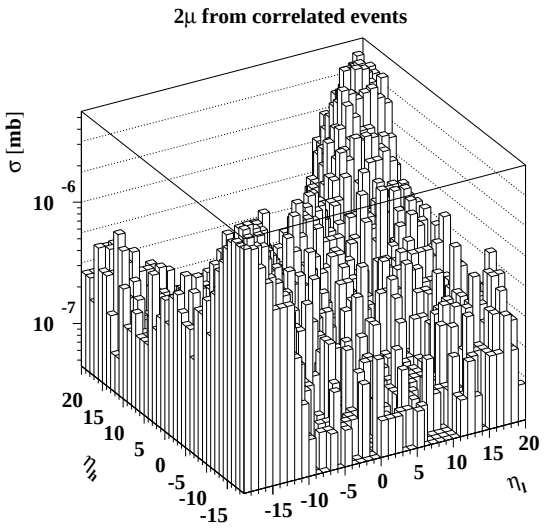

Figure 37: Dependence between η of lower and higher p_t muons for correlated events in the case of $p_t^{cut} = 1$ GeV.

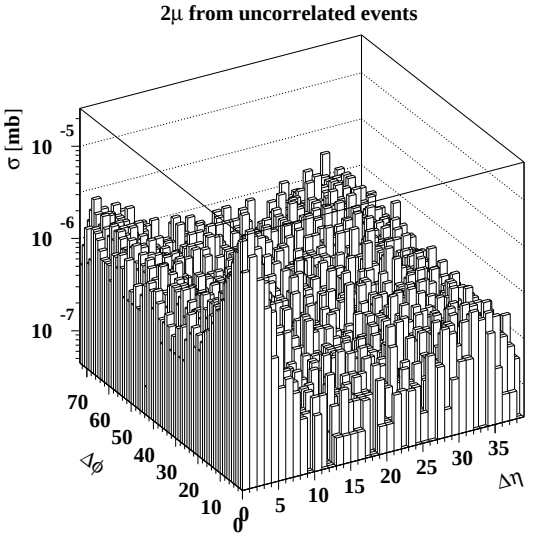

Figure 38: Dependence between $\Delta\eta$ and $\Delta\phi$ for uncorrelated events in the case of $p_t^{cut} = 1$ GeV.

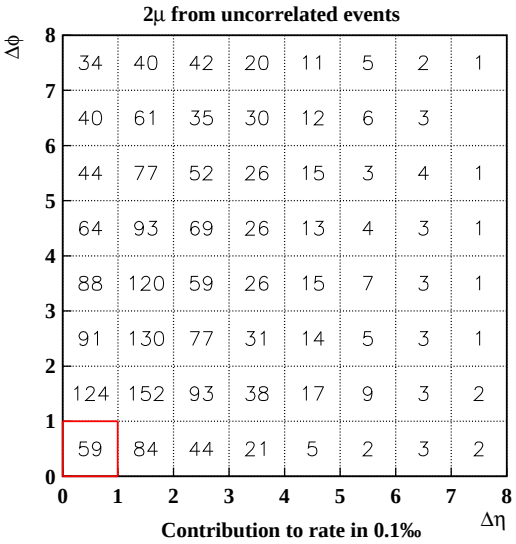

Figure 39: Contributions to the uncorrelated rate from the region of small differences in η and ϕ for $p_t^{cut} = 1$ GeV.

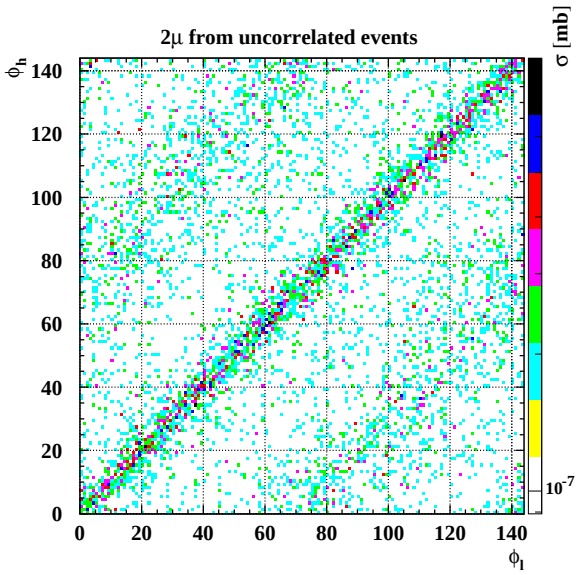

Figure 40: Dependence between ϕ of lower and higher p_t muons for uncorrelated events in the case of $p_t^{cut} = 1$ GeV.

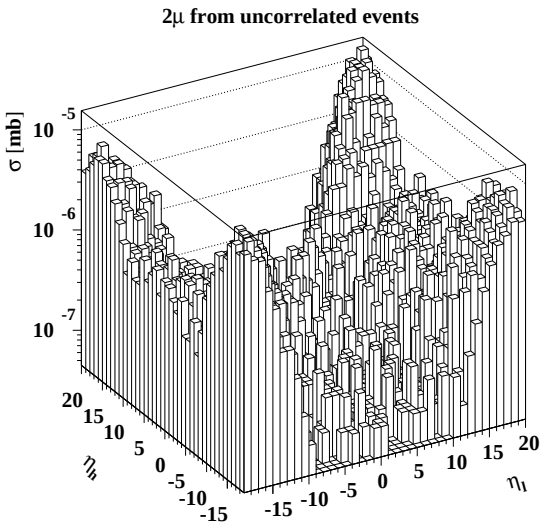

Figure 41: Dependence between η of lower and higher p_t muons for uncorrelated events in the case of $p_t^{cut} = 1$ GeV.

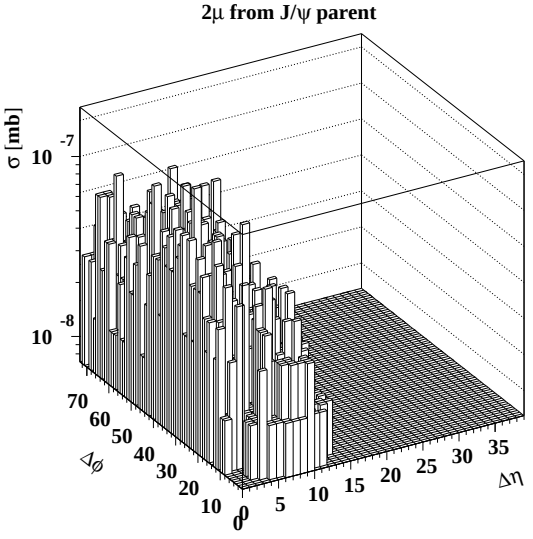

Figure 42: Dependence between $\Delta\eta$ and $\Delta\phi$ for J/ψ in the case of $p_t^{cut} = 1$ GeV.

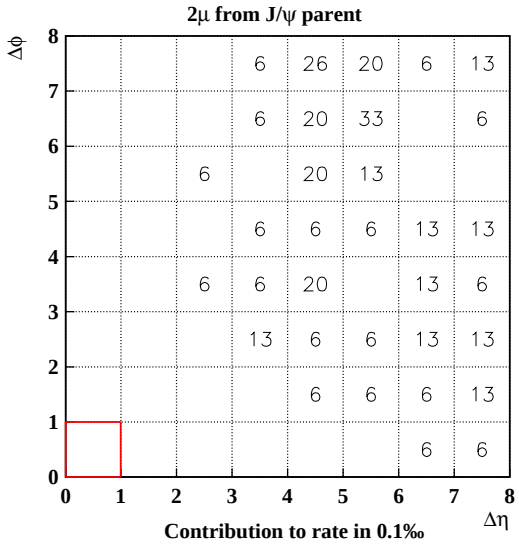

Figure 43: Contributions to the J/ψ rate from the region of small differences in η and ϕ for $p_t^{cut} = 1$ GeV.

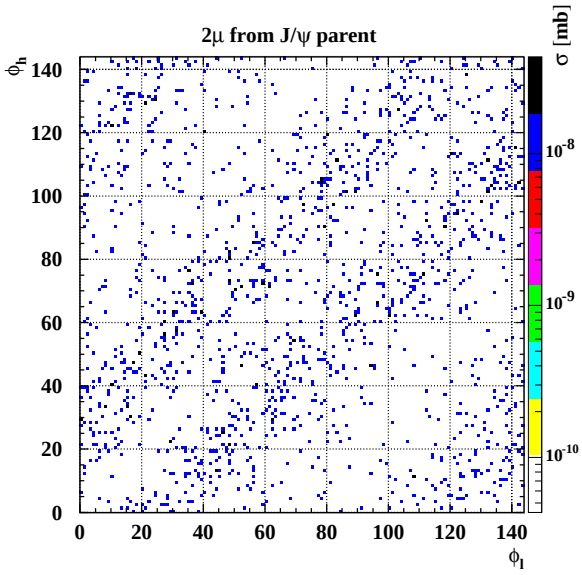

Figure 44: Dependence between ϕ of lower and higher p_t muons for J/ψ events in the case of $p_t^{cut} = 1$ GeV.

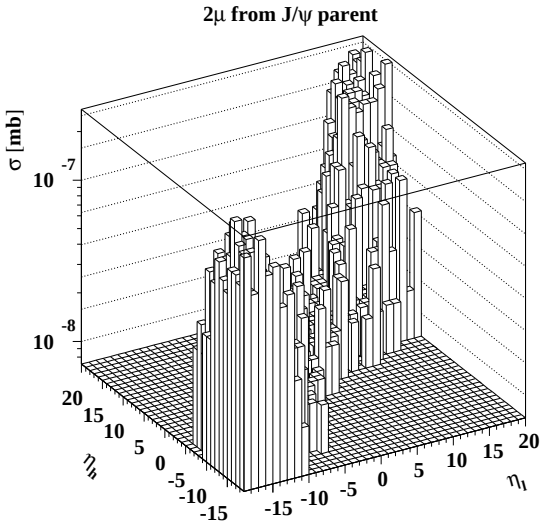

Figure 45: Dependence between η of lower and higher p_t muons for J/ψ events in the case of $p_t^{cut} = 1$ GeV.

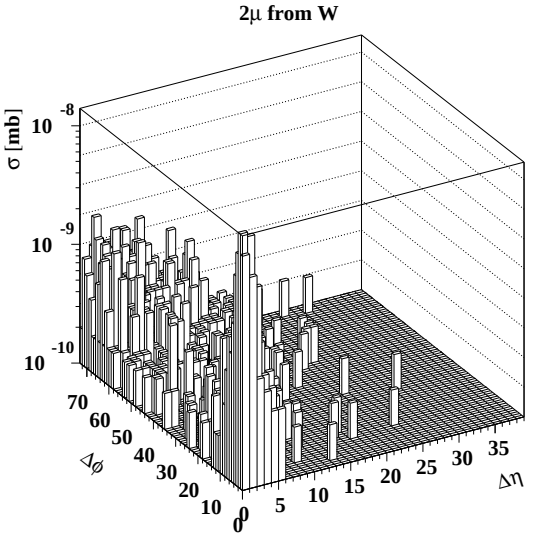

Figure 46: Dependence between $\Delta\eta$ and $\Delta\phi$ for W in the case of $p_t^{cut} = 1$ GeV.

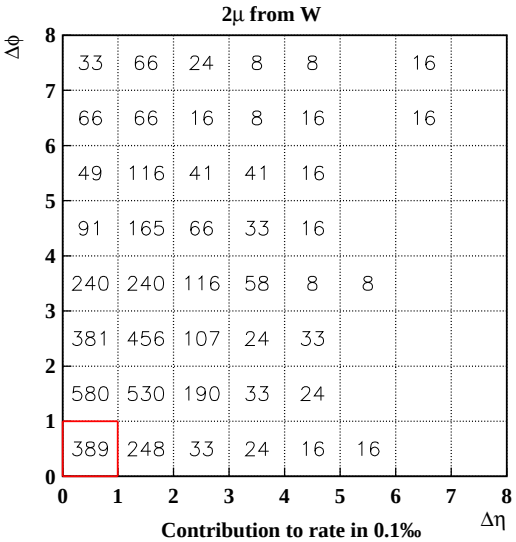

Figure 47: Contributions to the W rate from the region of small differences in η and ϕ for $p_t^{cut} = 1$ GeV.

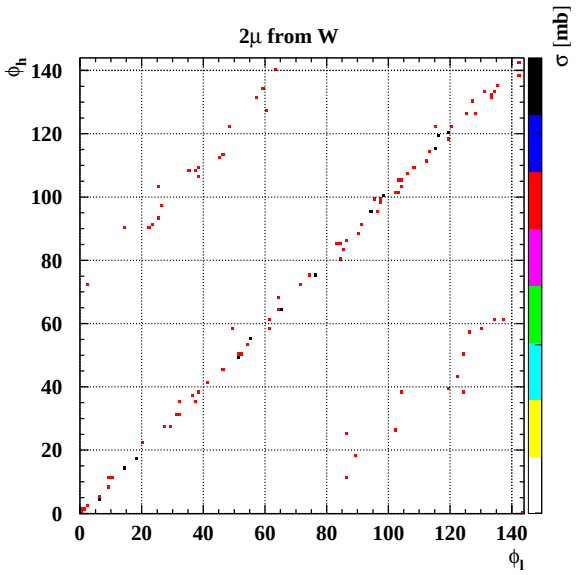

Figure 48: Dependence between ϕ of lower and higher p_t muons for W events in the case of $p_t^{cut} = 1$ GeV.

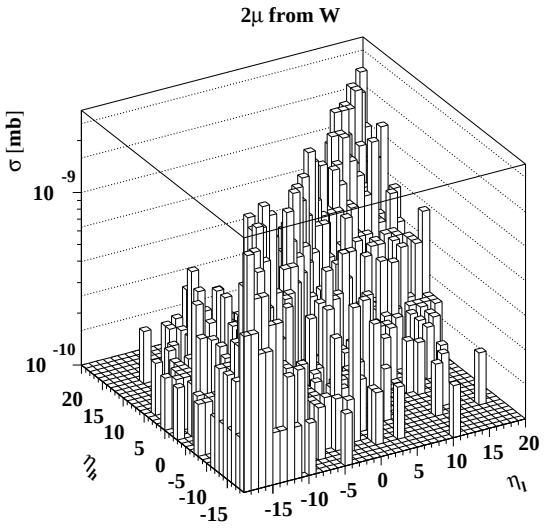

Figure 49: Dependence between η of lower and higher p_t muons for W events in the case of $p_t^{cut} = 1$ GeV.

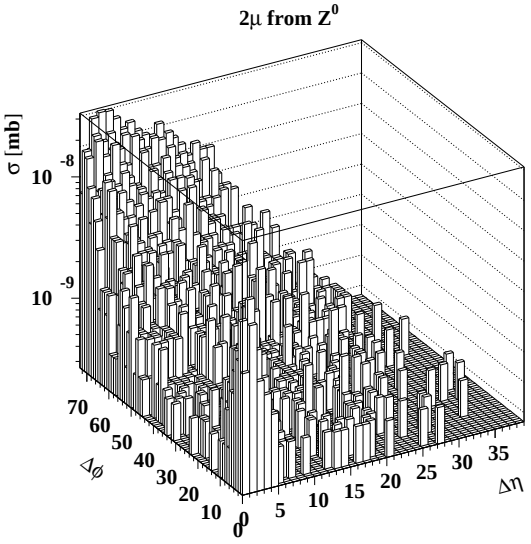

Figure 50: Dependence between $\Delta\eta$ and $\Delta\phi$ for Z^0 in the case of $p_t^{cut} = 1$ GeV.

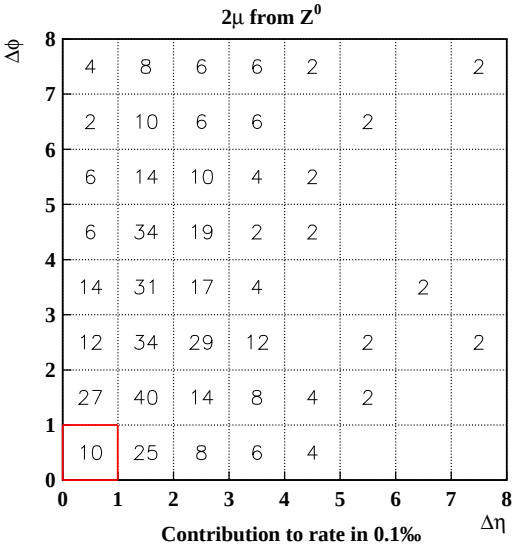

Figure 51: Contributions to the Z^0 rate from the region of small differences in η and ϕ for $p_t^{cut} = 1$ GeV.

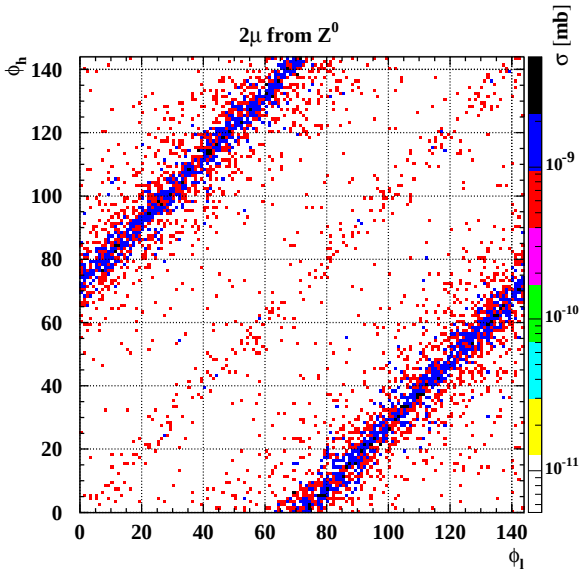

Figure 52: Dependence between ϕ of lower and higher p_t muons for Z^0 events in the case of $p_t^{cut} = 1$ GeV.

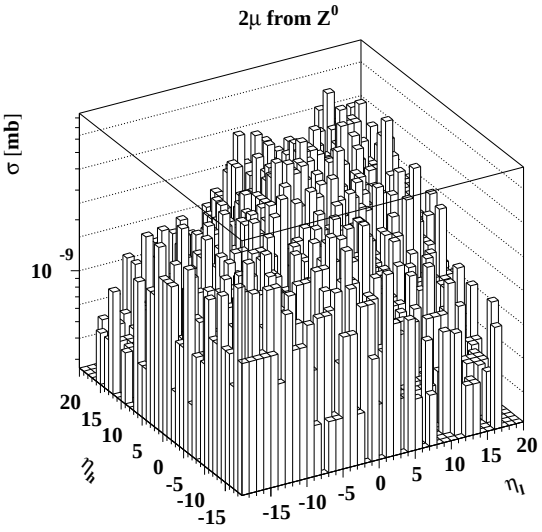

Figure 53: Dependence between η of lower and higher p_t muons for Z^0 events in the case of $p_t^{cut} = 1$ GeV.

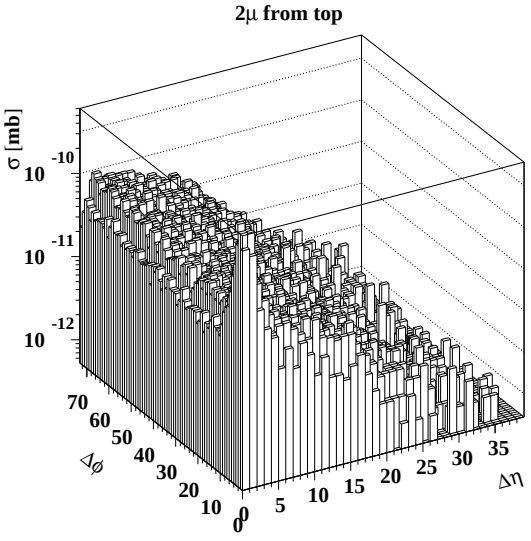

Figure 54: Dependence between $\Delta\eta$ and $\Delta\phi$ for top in the case of $p_t^{cut} = 1$ GeV.

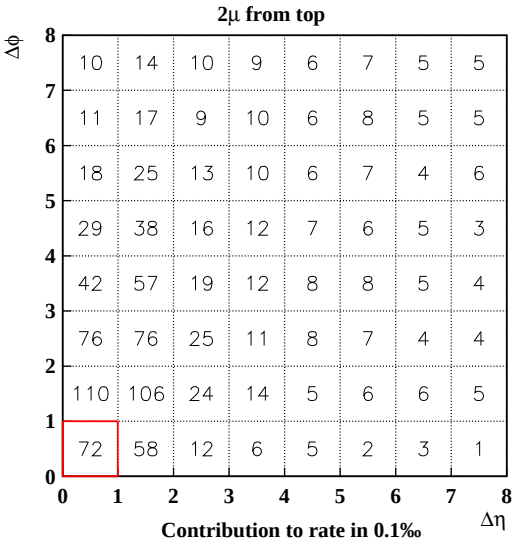

Figure 55: Contributions to the top rate from the region of small differences in η and ϕ for $p_t^{cut} = 1$ GeV.

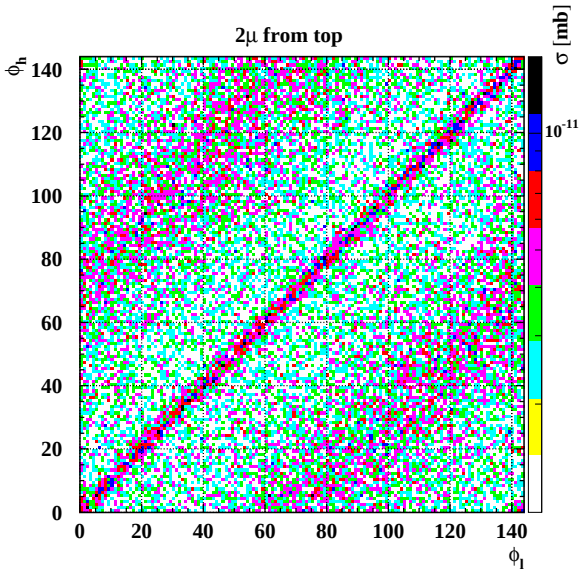

Figure 56: Dependence between ϕ of lower and higher p_t muons for top events in the case of $p_t^{cut} = 1$ GeV.

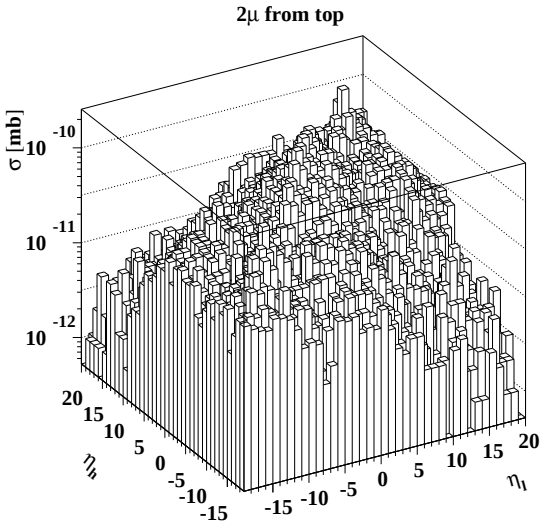

Figure 57: Dependence between η of lower and higher p_t muons for top events in the case of $p_t^{cut} = 1$ GeV.

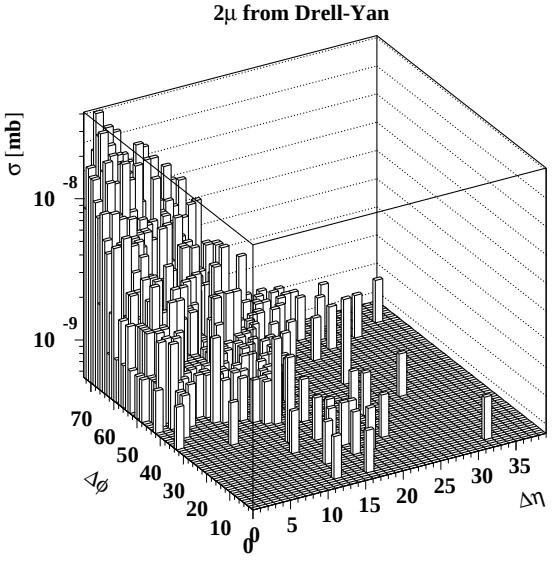

Figure 58: Dependence between $\Delta\,\eta$ and $\Delta\,\phi$ for Drell-Yan in the case of $p_t^{cut} = 1$ GeV.

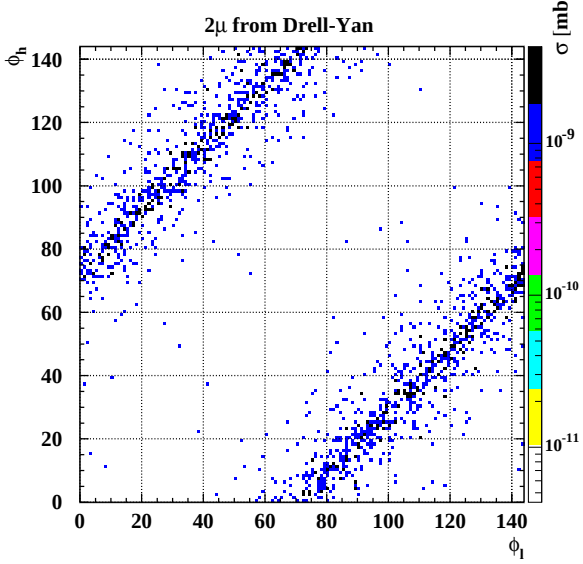

Figure 59: Dependence between ϕ of lower and higher p_t muons for Drell-Yan events in the case of $p_t^{cut} = 1$ GeV.

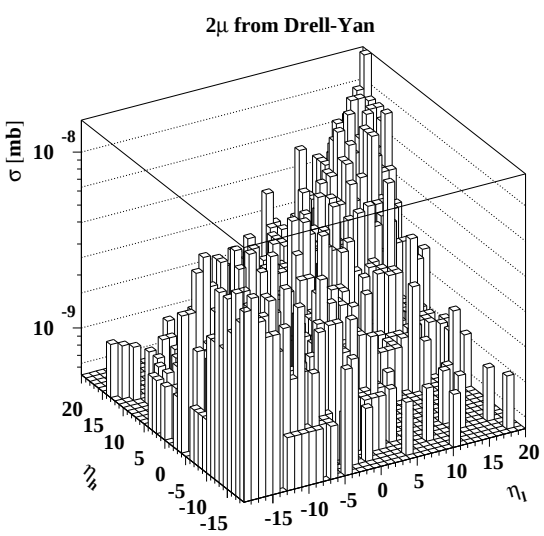

Figure 60: Dependence between η of lower and higher p_t muons for Drell-Yan events in the case of $p_t^{cut} = 1$ GeV.

The main impressions coming from these Figs. are

- Minimum bias events are collected mostly in forward regions due to soft p_t spectra. In correlated events both μ appear mostly in the same hemisphere, in uncorrelated events there is also significant contribution of opposite directions. The rise of the p_t cut to 4 GeV causes focusing of the sample in the region low $\Delta\phi$, $\Delta\eta$ differences.

- In J/ψ decays we have to deal with both μ in the same η region, but no part of the rate is lost – empty red square. The things may go worst when magnetic field applied – opposite signs μ may point into the same sector in the reference station – so called "cowboy events". The $p_t^{cut} = 4$ GeV introduces even stronger changes than for minimum bias.

- Muons from W appear with small differences in η.

- For Drell–Yan and Z^0 the distributions are concentrated around high differences in ϕ and small in η.

- Distribution of muons from top is rather flat in $\Delta\phi$ and smoothly falls down with the rise of $\Delta\eta$.

- The biggest rejection of events due to both μ pointing in the same ϕ and η sector was ascertained for W.

The short resume of the $\Delta\eta$ vs $\Delta\phi$ figures is given in Tables 7 – 10. The towers/sectors were grouped by three in η and by five in ϕ, to reduce the statistical fluctuations. The rise of p_t^{cut} to 4 GeV introduce significant changes only for minimum bias and J/ψ.

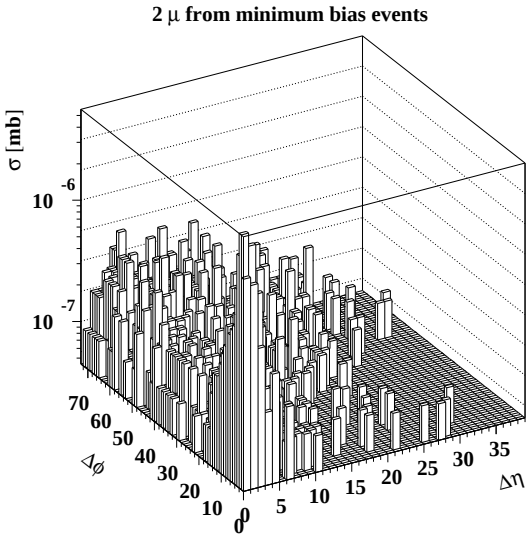

Figure 61: Dependence between $\Delta\eta$ and $\Delta\phi$ for minimum bias events in the case of $p_t^{cut} = 4$ GeV.

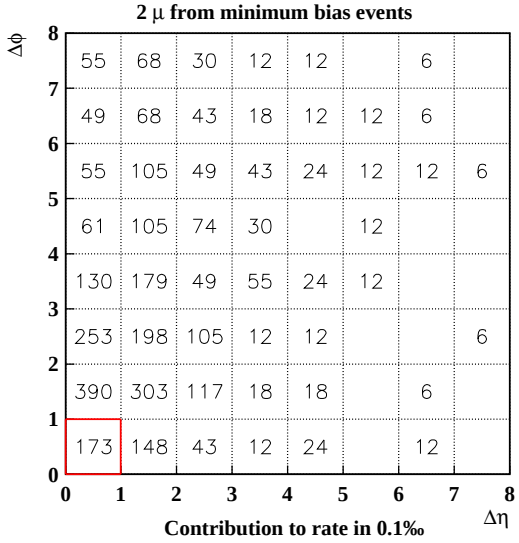

Figure 62: Contributions to the minimum bias rate from the region of small differences in η and ϕ for $p_t^{cut} = 4$ GeV.

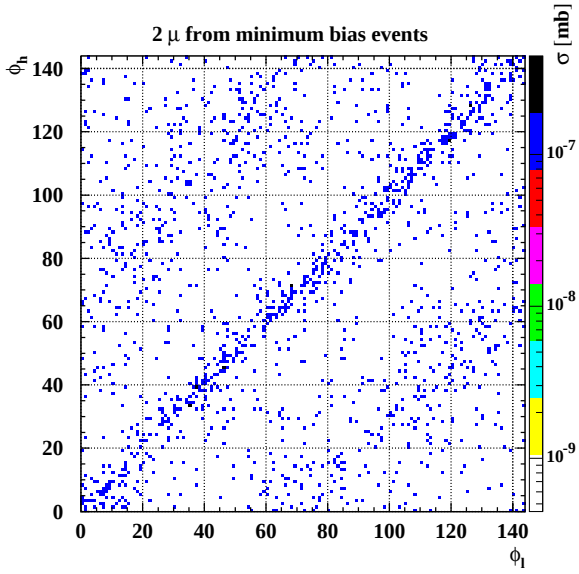

Figure 63: Dependence between ϕ of lower and higher p_t muons for minimum bias events in the case of $p_t^{cut} = 4$ GeV.

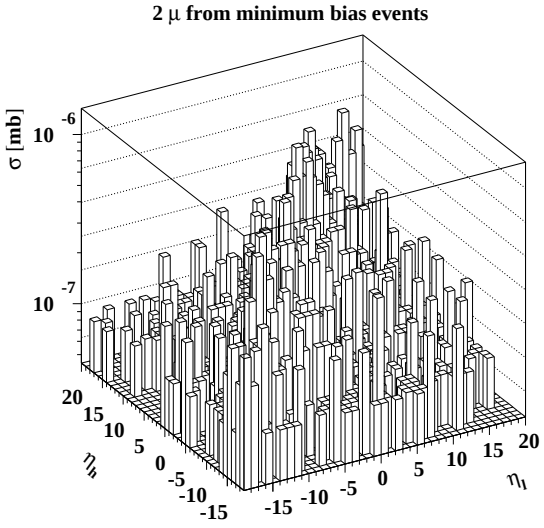

Figure 64: Dependence between η of lower and higher p_t muons for minimum bias events in the case of $p_t^{cut} = 4$ GeV.

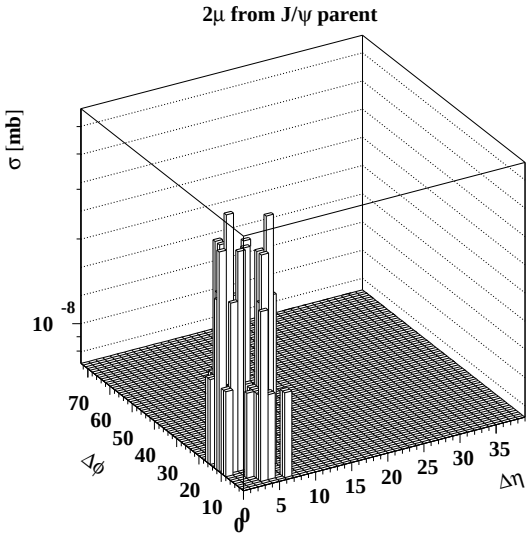

Figure 65: Dependence between $\Delta\,\eta$ and $\Delta\,\phi$ for J/ψ in the case of $p_t^{cut} = 4$ GeV.

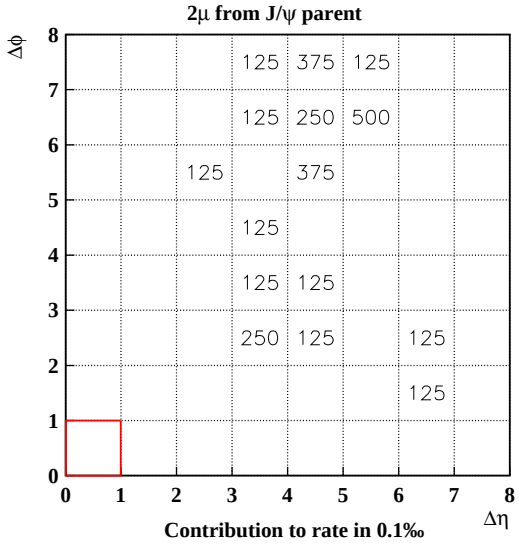

Figure 66: Contributions to the J/ψ rate from the region of small differences in η and ϕ for $p_t^{cut} = 4$ GeV.

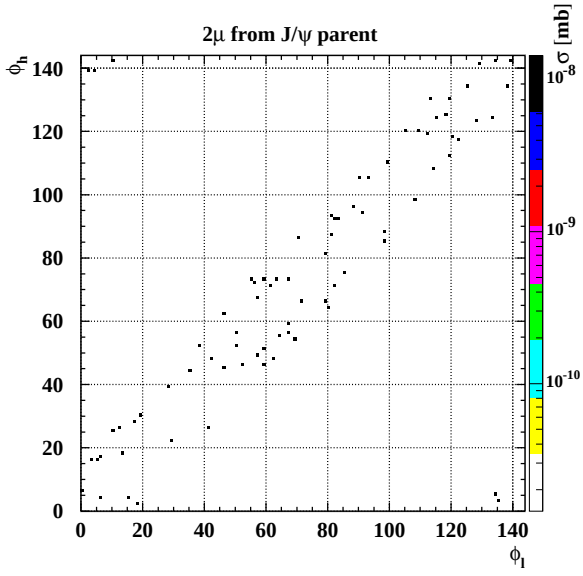

Figure 67: Dependence between ϕ of lower and higher p_t muons for J/ψ events in the case of $p_t^{cut} = 4$ GeV.

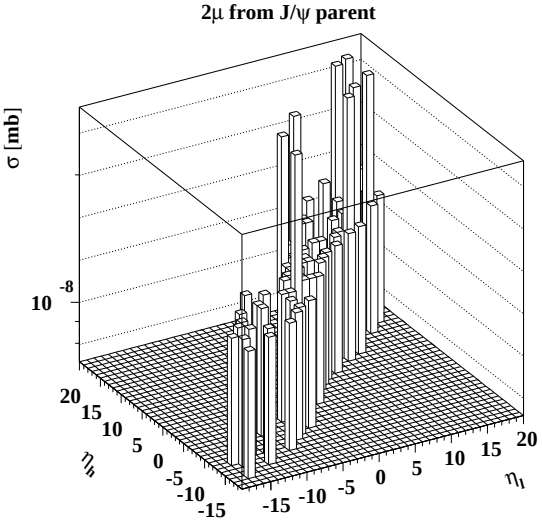

Figure 68: Dependence between η of lower and higher p_t muons for J/ψ events in the case of $p_t^{cut} = 4$ GeV.

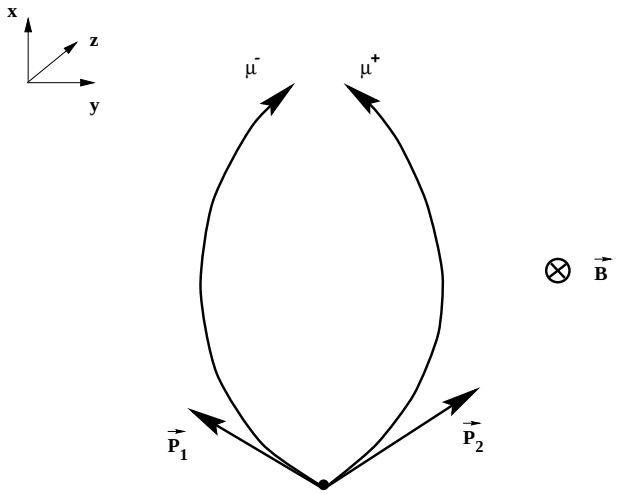

Figure 69: "Cowboy event"

Source of muons	Range in $\Delta\eta$												
	1	2	3	4	5	6	7	8	9	10	11	12	13
2μ from minbias events	38	18	7	4	4	3	3	2	3	4	6	5	3
2μ from correlated events	45	24	9	5	4	3	2	2	1	1	2	1	1
2μ from uncorrelated events	35	15	5	3	4	3	3	3	4	6	8	8	3
2μ from J/ψ parent	47	34	14	4	1	0	0	0	0	0	0	0	0
2μ from W	59	17	9	7	4	2	1	1	0	0	0	0	0
2μ from Z^0	22	20	17	15	10	8	4	2	1	1	0	0	0
2μ from top	28	22	16	12	9	6	3	2	1	1	0	0	0
2μ from Drell-Yan	33	27	17	11	7	4	1	0	0	0	0	0	0

Table 7: Percentage contribution of different $\Delta\eta$ ranges to the double μ rates of a specific type ($p_t^{cut} = 1$ GeV)

Source of muons	Range in $\Delta\phi$														
	1	2	3	4	5	6	7	8	9	10	11	12	13	14	15
2μ from minbias events	18	12	7	5	4	4	4	4	5	5	6	6	7	8	5
2μ from correlated events	19	14	8	6	4	4	4	4	4	5	5	6	6	7	4
2μ from uncorrelated events	18	10	6	5	4	4	4	4	5	5	6	7	8	9	5
2μ from J/ψ parent	3	5	8	11	11	15	11	11	6	5	4	3	4	2	1
2μ from W	42	8	2	1	1	1	1	1	1	2	3	4	8	15	10
2μ from Z^0	4	2	1	1	1	1	1	1	2	2	4	6	12	28	34
2μ from top	11	6	5	5	5	5	6	6	6	7	7	8	9	9	5
2μ from Drell-Yan	0	0	0	0	0	0	0	1	2	3	5	8	13	33	35

Table 8: Percentage contribution of different $\Delta\phi$ ranges to the double μ rates of a specific type ($p_t^{cut} = 1$ GeV)

Source of muons	Range in $\Delta\eta$												
	1	2	3	4	5	6	7	8	9	10	11	12	13
2μ from minbias events	46	20	10	7	7	3	2	2	2	1	0	0	0
2μ from correlated events	48	21	10	6	6	3	2	2	1	1	0	0	0
2μ from uncorrelated events	40	14	9	10	8	5	4	3	4	2	1	0	0
2μ from J/ψ parent	48	47	5	0	0	0	0	0	0	0	0	0	0
2μ from W	57	13	13	10	4	2	1	0	0	0	0	0	0
2μ from Z^0	20	20	17	15	11	8	5	2	1	1	0	0	0
2μ from top	28	22	17	13	9	6	3	1	1	0	0	0	0
2μ from Drell-Yan	27	26	19	13	10	4	1	0	0	0	0	0	0

Table 9: Percentage contribution of different $\Delta\eta$ ranges to the double μ rates of a specific type ($p_t^{cut} = 4$ GeV)

Source of muons	Range in $\Delta\phi$														
	1	2	3	4	5	6	7	8	9	10	11	12	13	14	15
2μ from minbias events	27	11	5	3	2	2	3	3	4	4	6	6	8	10	6
2μ from correlated events	25	13	5	4	2	2	3	4	4	4	6	6	8	9	5
2μ from uncorrelated events	31	5	3	2	1	2	3	2	4	5	6	8	9	11	8
2μ from J/ψ parent	10	35	39	16	0	0	0	0	0	0	0	0	0	0	0
2μ from W	42	2	1	1	0	0	1	1	1	1	2	6	11	18	13
2μ from Z^0	2	1	0	0	1	0	1	1	2	3	4	6	13	30	36
2μ from top	11	5	5	5	5	5	6	6	6	7	7	8	9	10	5
2μ from Drell-Yan	0	0	0	0	0	0	0	1	2	3	6	8	13	30	37

Table 10: Percentage contribution of different $\Delta\phi$ ranges to the double μ rates of a specific type ($p_t^{cut} = 4$ GeV)

5 Simulation of detector response on 2μ events

5.1 Description of muon processing procedure

Before discussion of trigger rates few words should be dedicated to muons propagation. For muons coming almost directly from vertex of p-p collision no tricks were needed. Such μ were coming, for example, from the direct beauty or charm particle decay, which takes place on the first few millimetres from the production vertex, even for the Lorentz boost of the order ten. Extra treatment was applied to events in which a μ comes from the $K^{\pm}$ or $\pi^{\pm}$ decay, which may happen even few meters from the collision vertex. In the first step hadron was tracked. When length of its track was equal to the value obtained during Pythia generation, it was checked whether the decay vertex was inside the tracker volume.

If *YES*, the further meson tracking was skipped and μ tracking from the vertex different from given by Pythia, on account of magnetic field, began. But before tracking, a new direction of muon momentum vector was calculated. The old μ momentum vector was rotated to preserve its orientation in respect to decaying kaon or pion momentum vector. If considered hadron reached calorimeter, then the muon coming from its decay was not tracked. Such treatment implies that obtained results – rate and correlations – are the best approximation of these expected during experiment.

5.2 The 2μ trigger rates

Double μ rates presented in this section are thus trigger rates. Every μ had to leave hits in at least 3 stations, while with the geometrical acceptance procedure, used earlier, reaching 2 high p_t station was sufficient. These 3 or 4 "fired" strips should form a pattern, which could be found among predefined ones. Therefore, some reduction in the comparison to accepted rates may be expected, especially for the minimum bias or J/ψ samples, where μ spectra were soft.

Figs. 70 and 71 directly correspond to these presented in section 3. Conclusions coming from comparing these Figs. are as follows

- Trigger rates at 1 GeV are lower than accepted ones – about 4 kHz of the total rate. In the range 4 – 20 GeV the agreement of the trigger and accepted rates is good.
- Reduction of the rate is the strongest for minimum bias and J/ψ events. Soft μ have got the problems to score hits in at least three stations. There may also happen a problem with the formation of the patern, if fired strips belong to different cones.
- The division on minimum bias rate dominant at low p_t and Z^0 at high p_t is preserved.
- Rate curves became more flat in high p_t region – trigger p_t reconstruction procedure generally gives higher value than original. The greatest shift happens for muons with p_t over 40 GeV.

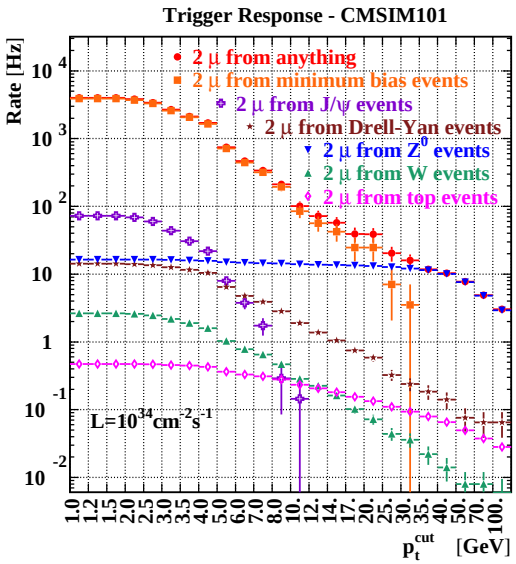

Figure 70: The 2μ rates from all sources. Trigger response obtained with MRPC package.

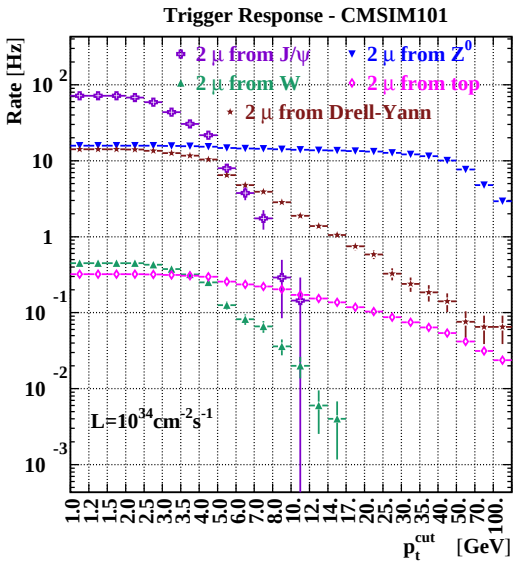

Figure 71: The 2μ rates from "heavy" sources. Trigger response obtained with MRPC package.

- Probably there is no need to preserve four bins in the range $p_t^{cut} < 2.5$ GeV, because the rate curves are flat in this range for all cases.

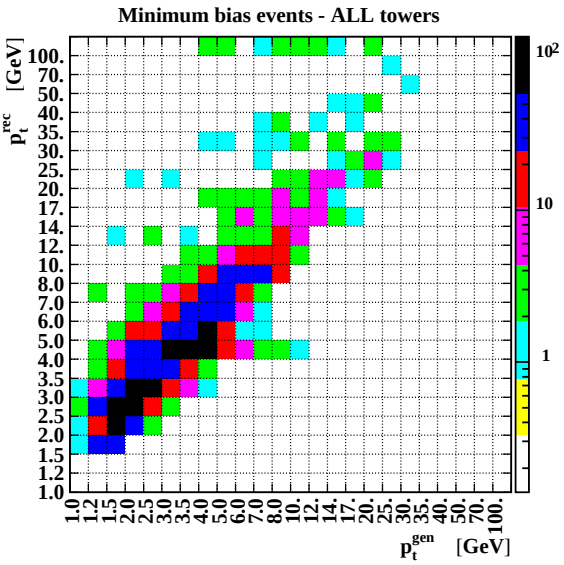

Figure 72: Comparison between p_t^{gen} and p_t^{rec} in minimum bias events for all η towers

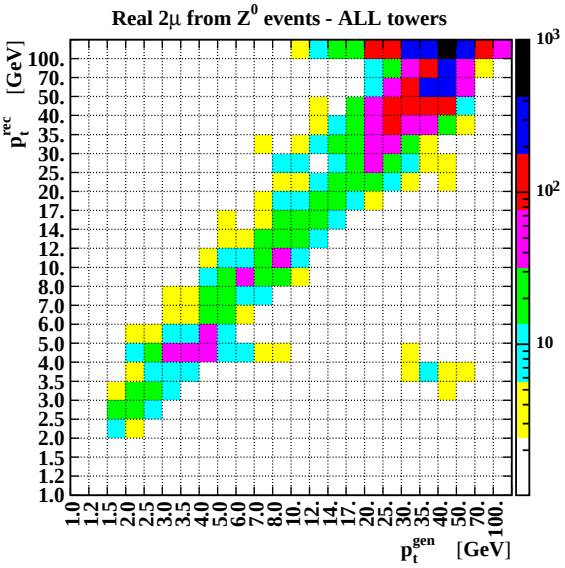

Figure 73: Comparison between p_t^{gen} and p_t^{rec} in Z^0 events for all η towers

Fig. 72 – 73 present comparison between the generated p_t of the μ and reconstructed by the trigger algorithm. Concentration over diagonal may be ascertained. It looks that the overestimate of p_t in Z^0 events happens more often and is generally greater than in minimum bias. The main impression is that the most significant overestimate of p_t comes from rather hard muons. The limited resolution of the RPC plays important role there. To account for that we had to introduce much larger bins in that p_t range - there are sixteen

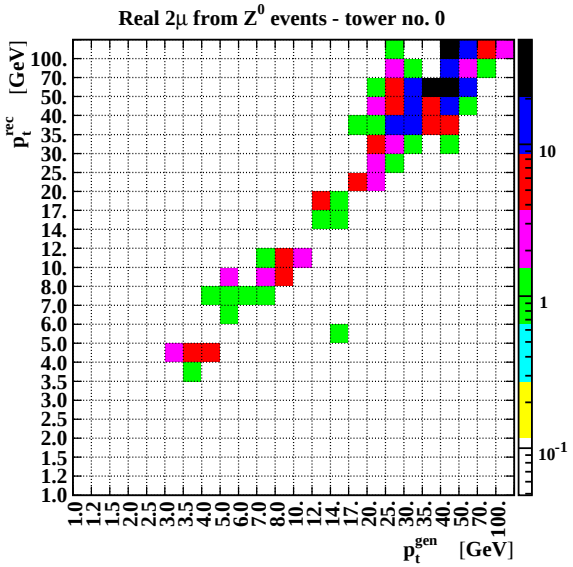

Figure 74: Comparison between p_t^{gen} and p_t^{rec} in Z^0 events for η tower no. 0

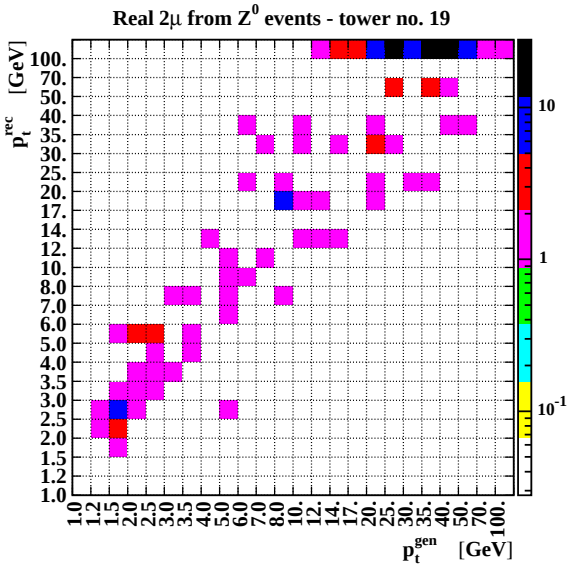

Figure 75: Comparison between p_t^{gen} and p_t^{rec} in Z^0 events for η tower no. 19

bins up to $p_t = 20$ GeV and only eight above this value. We had to divide transverse momentum scale of our trigger into small number of high p_t bins. Figs. 74 – 75 for the most central tower, and for the most forward one, prove that the largest overestimate of p_t happens in forward direction. The reason probably lies in the shape of magnetic field in the forward region. Most of the track bending in this area is done between the first and the second muon stations. Behind the second μ station in forward direction, magnetic field turns back through the yoke. Additionally, longitudinal component of the momentum is much larger than transverse component in this region. In this case, tracks are very similar to straight line. Therefore the influence of the field is not big enough to cause large differences between "fired" strips, which results in triggering for high p_t.

Figs. 76 – 81, presenting different subcategories of minimum bias rates were also given. As one could expect the dominance of so called correlated events is now more clear. Beauty decays seem to preserve their dominance over other categories. Cascade decays still have significant contribution.

The last Figs. in this section (82 – 83) are dedicated to the quality of the pseudorapidity reconstruction. It was done for two types of μ spectrum – soft from minimum bias and hard from Z^0 decays. For the perfect reconstruction, the diagonal should be occupied. It is nearly true. It seems that, on average, the reconstructed η is slightly shifted towards higher absolute value than the input one. It is a natural consequence of bending in magnetic field, due to which a track crosses boundaries between towers. It can be said that under field influence a muon approaches the beam axis. Ideally it moves on the spiral, and its rotation axis is parallel to the p-p beams. When the track is more similar to the straight line (muons with large transverse momentum) passing between towers is less likely. Therefore, the departure from the diagonal seems to be much greater for the minimum bias than for the Z^0 events.

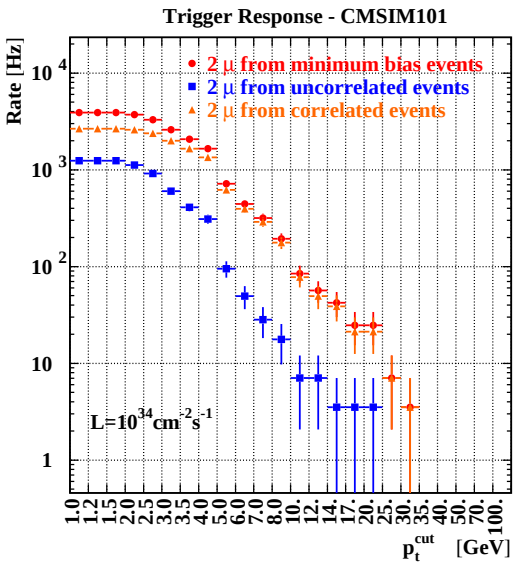

Figure 76: The 2μ rates from correlated and uncorrelated categories in minimum bias. Trigger response obtained with MRPC package.

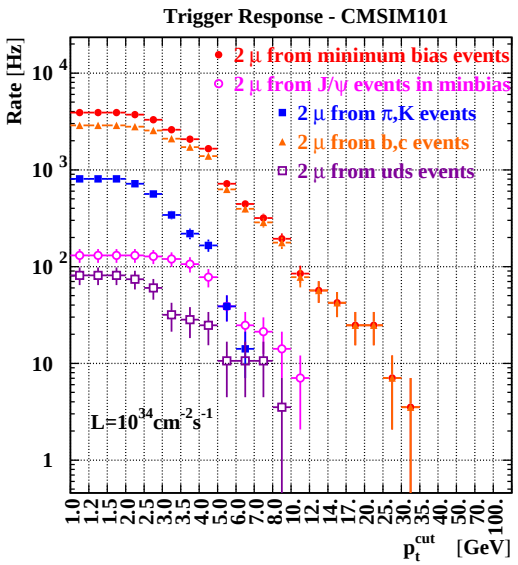

Figure 77: The 2μ rates from different categories in minimum bias. Trigger response obtained with MRPC package.

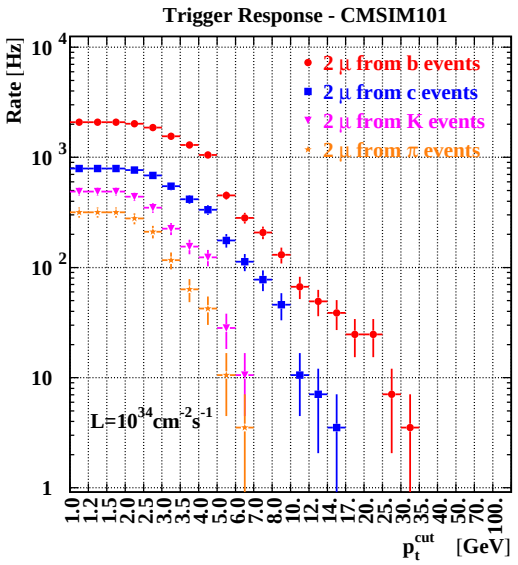

Figure 78: The 2μ rates from different categories in minimum bias. Trigger response obtained with MRPC package.

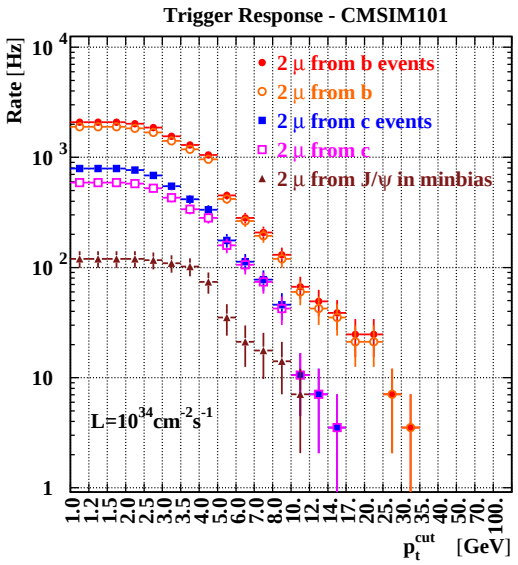

Figure 79: The 2μ rates from different categories in minimum bias. Trigger response obtained with MRPC package.

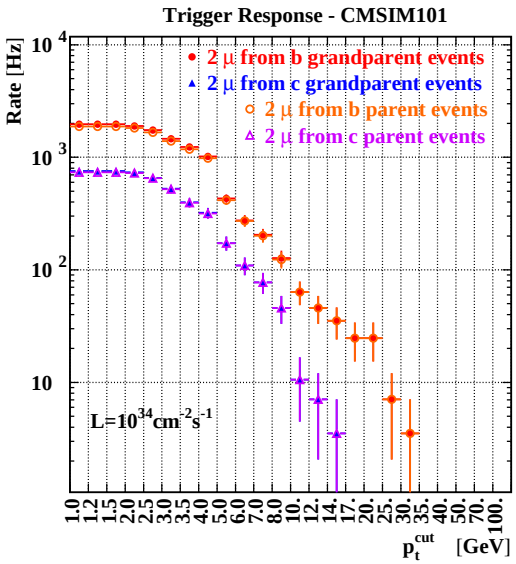

Figure 80: The 2μ rates from different categories in minimum bias. Trigger response obtained with MRPC package.

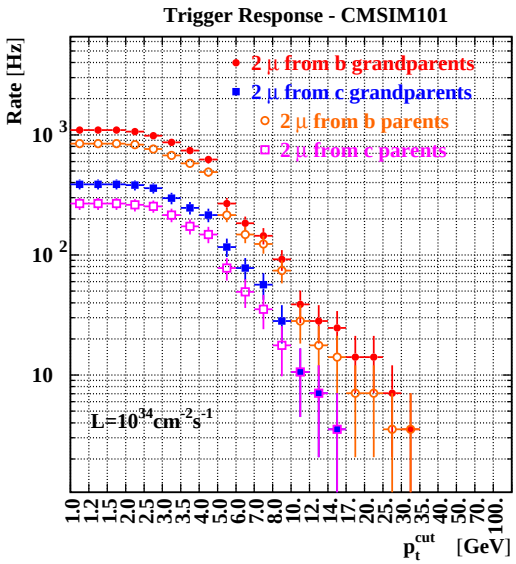

Figure 81: The 2μ rates from different categories in minimum bias. Trigger response obtained with MRPC package.

It should be stressed that this effect is unavoidable, but it does not seem very significant.

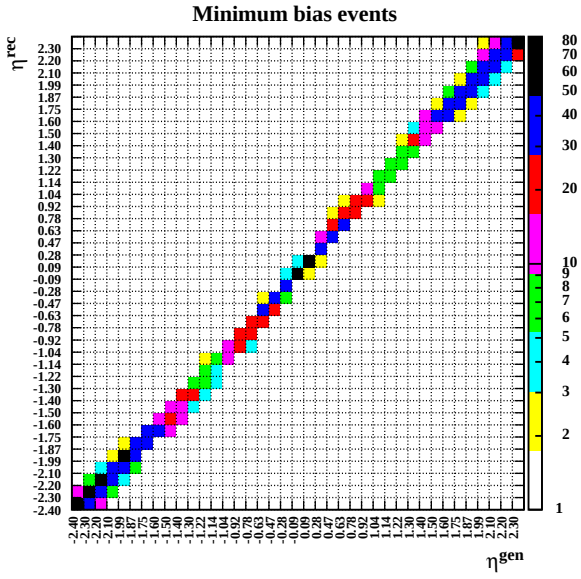

Figure 82: Dependence between η_t^{gen} and η_t^{rec} in minimum bias events

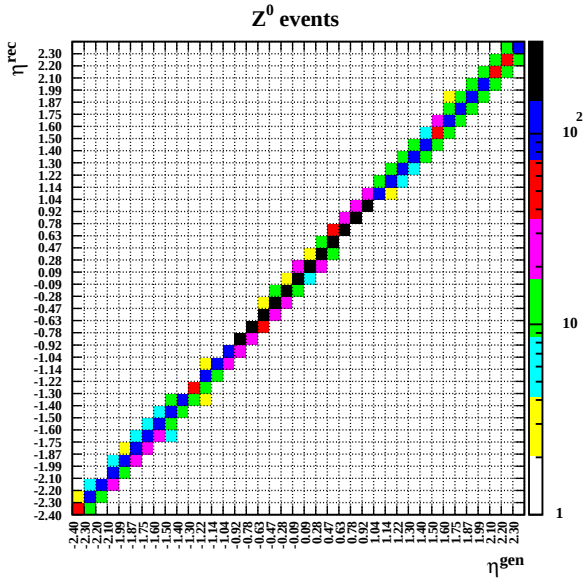

Figure 83: Dependence between η_t^{gen} and η_t^{rec} in Z^0 events

5.3 The fake 2μ trigger rates

Fig. 84 presents a single μ trigger rate. It is to be compared with the accepted single muons rate shown in Fig. 25. The reduction of the rate for the soft muons is caused by small detection efficiency for soft μ's. After the experience with overestimate of p_t we are not surprised with some flattening of a single μ rate, and, as the consequence, also 2μ

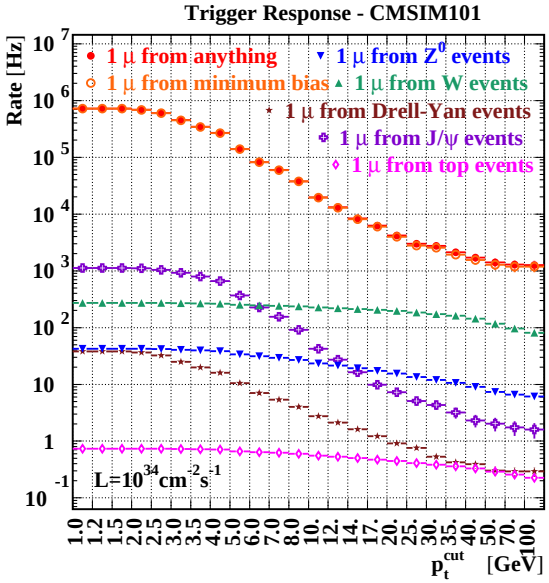

Figure 84: Single μ rates from all generations

fake rate. Minimum bias single μ rate dominates over other ones at least by one order of magnitude in the full p_t range. Figs. 85 and 86 compare total real and fake rates for $L = 10^{34}\text{cm}^{-2}\text{s}^{-1}$ and $L = 10^{33}\text{cm}^{-2}\text{s}^{-1}$ respectively. Conclusions

- Fake rate can not be totally neglected for the highest luminosity in any p_t range.
- For the highest p_t cut, the purity of the double μ sample is about 98 – 99 % .
- Probably the lowest possible p_t cut (requesting to give at least 95 % purity) will be about 12–20 GeV in the highest luminosity case.
- Due to the fact that $RATE_{fake} \propto L^2$ in the case $L = 10^{33}\text{cm}^{-2}\text{s}^{-1}$ the proportions are ten times better.

Additionally the ratios between the double and single μ rates at 1 and 4 GeV are presented in Table 11. This Table is done only for these categories of events in which the direct decay into two muons is possible.

Source of the muon events	Double rate : Single rate at 1 GeV	Double rate : Single rate at 4 GeV
J/ψ events	1 : 12	1 : 20
Z^0 events	1 : 2	1 : 2
Drell-Yan events	1 : 2	1 : 2

Table 11: The ratio between double and single muon rates for $p_t^{cut} = 1$ and $p_t^{cut} = 4$ GeV.

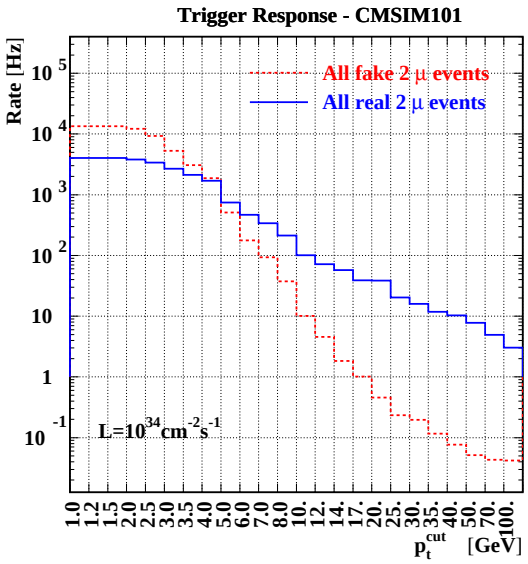

Figure 85: Total real and fake trigger rates for $L = 10^{34}\text{cm}^{-2}\text{s}^{-1}$

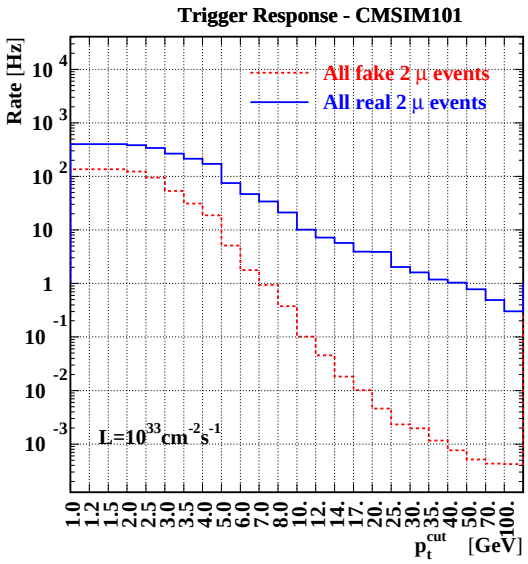

Figure 86: Total real and fake trigger rates for $L = 10^{33}\text{cm}^{-2}\text{s}^{-1}$

5.4 Comparison between the real and the ghost rates

It was established that unavoidable feature of our trigger algorithm is a ghost production. That means the recognition of a single μ as several trigger candidates. Unfortunately, for the version of algorithm discussed here, that probability is greater than for real double μ events. Total ghost and real 2 μ rate are presented on Fig. 87, whereas contributions to the ghost one on Fig. 87.

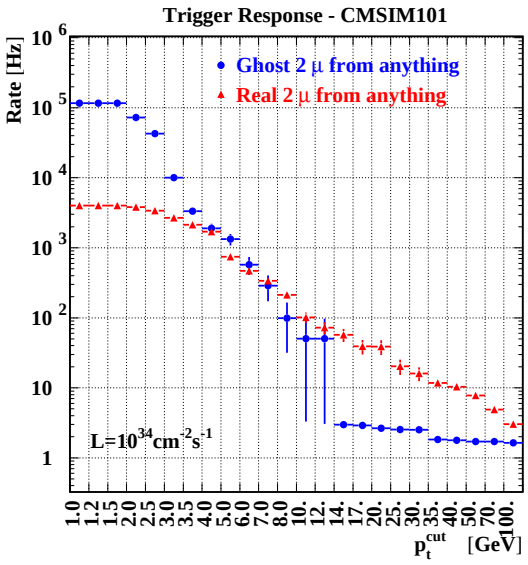

Figure 87: Total ghost and real trigger rates for $L = 10^{34}\text{cm}^{-2}\text{s}^{-1}$

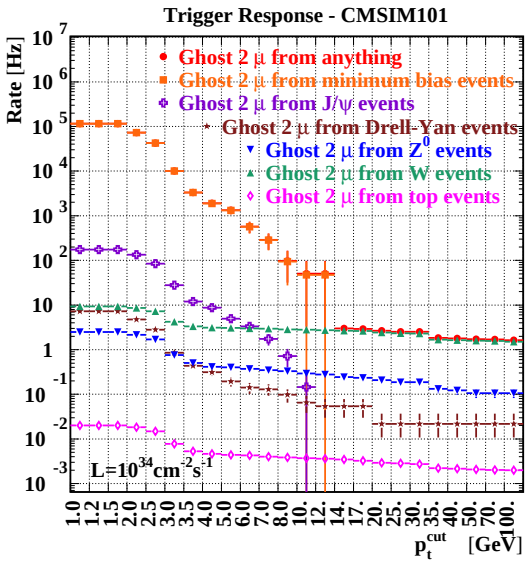

Figure 88: Contributions to ghost rate for $L = 10^{34}\text{cm}^{-2}\text{s}^{-1}$

Impressions coming from these Figs.

- Ghost rate exceeds real one for low p_t cuts. The rates are in balance in wide range up to dozen GeV.

- There are two major sources of ghost rate – minimum bias at low and moderate p_t range and W in high p_t range.

The ratios between different types of the real and ghost 2 μ rates at 1 GeV and 4 GeV are presented in Table 12.

Source of 2μ events	Real rate : Ghost rate at 1 GeV	Real rate : Ghost rate at 4 GeV
Minimum bias events	1 : 25	1 : 1
J/ψ events	1 : 2	25 : 10
W events	1 : 3	2 : 3
Z^0 events	10 : 1	30 : 1
top events	20 : 1	100 : 1
Drell-Yan events	2 : 1	30 : 1

Table 12: The ratio between the real and ghost rates for $p_t^{cut} = 1$ and $p_t^{cut} = 4$ GeV.

It was ascertained that ghost events happen only in forward regions $|\eta| > 1.0$ and the most of them in the range $2.0 < |\eta| < 2.4$. No ghost events were found in the barrel. The reason of ghost concentration in a forward direction, lies in smaller angular range of η towers – Fig. 5. Most of the ghost rate is caused by soft μ because the track of a such μ can cross more ϕ sectors and be visible in more cones.

There is no doubt that on this stage of the algorithm development total ghost 2 μ rate exceeds real one. These situation is unacceptable and the algorithm should be improved. An attempt to do so is presented in the next section, where the influence of enlargement of the veto area around μ trigger candidate on the reduction of real and suppresion of ghost rates will be considered.

5.5 Spatial separation between two μ tracks.

Let us concentrate on differences introduced to correlation of μ pairs, by magnetic field and multiple scattering. Figs. 89 – 99, correspond to these from section 4. Global view in the space of $\Delta\eta$ and $\Delta\phi$ and the zoom of small differences region were shown. When we compare the influence of the detector conditions with the situation discussed in section 3 it is

- positive for muons coming from minimum bias events, W, Z^0 and top decays – now separation of tracks is better.

- negative for muons from J/ψ decays – fraction of events with small differences is greater.

Most probably the worse situation for J/ψ is caused by the focusing negative and positive muons to the same segment. On zoom figures some area were marked with colours to study the influence of different concepts of vetoing on the reduction of the real 2 μ rate and getting rid of the ghost rate – Figs. 104 – 109. The ghost rate seems to be fundamentally the same for all classes of events. Empty region 2×2 around (0,0) is natural consequence of implemented veto in CMSIM101 algorithm. Very rarely, we have to deal with ghosts separated in ϕ more than 2 units – contribution of such events is on the level of few permille. Tables 13 and 14 encourage us to enlarge veto region up to 2 units both in ϕ and η. The ghost rate is then almost totally suppressed, and the real one stays above 95% of its value when no veto was applied[36]. Small reduction for W may be partially a statistical fluctuation. The biggest rejection – 4 % – was ascertained for J/ψ. It seems to be a reasonable price for excluding more than 99 % of the ghosts.

Source of 2μ events	Veto option		
	$\Delta\eta \leq 1$ and $\Delta\phi \leq 1$	$\Delta\eta \leq 1$ and $\Delta\phi \leq 2$	$\Delta\eta \leq 2$ and $\Delta\phi \leq 2$
Minimum bias events	99.2	98.7	98.5
J/ψ events	98.2	98.4	96.0
W events	99.6	99.1	98.7
Z^0 events	99.97	99.91	99.91
top events	99.8	99.5	99.2
Drell-Yan events	100	100	100

Table 13: Percentage of preserved real 2μ rate with different veto options

Source of 2μ events	Veto option	
	$\Delta\eta \leq 1$ and $\Delta\phi \leq 2$	$\Delta\eta \leq 2$ and $\Delta\phi \leq 2$
Minimum bias events	91.0	99.7
J/ψ events	88.4	99.9
W events	68.7	99.9
Z^0 events	83.2	100
top events	76.9	99.7
Drell-Yan events	87.5	100

Table 14: Percentage of ghost 2μ rate suppression with different veto options

[36] Percentage of the preserved real 2μ rate is counted with reference to definite type rate - even collected in region $\Delta\phi = 0$ and $\Delta\eta = 0$. Percentage of the ghost suppression refers to the ghost rate obtained with current veto procedure implemented in CMSIM101 – $\Delta\phi \leq 1$ and $\Delta\eta \leq 1$.

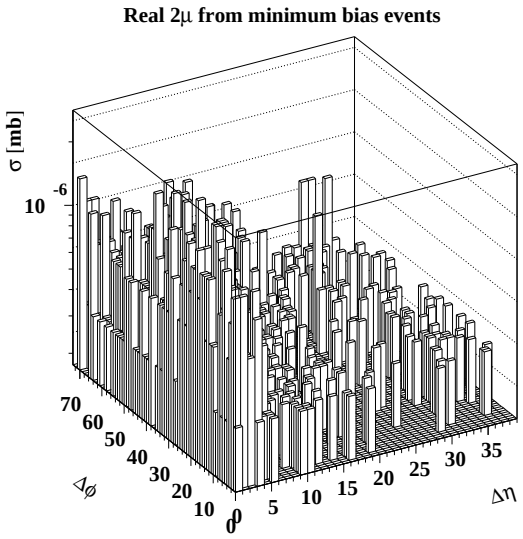

Figure 89: Dependence between $\Delta\eta$ and $\Delta\phi$ for muons from minimum bias events in the case of $p_t^{cut} = 1$ GeV – full trigger response.

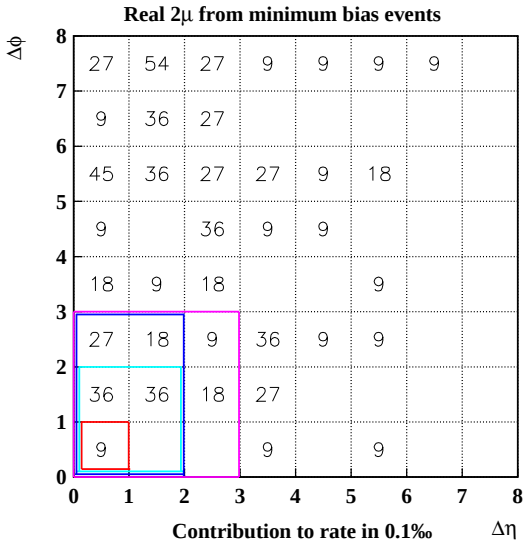

Figure 90: Contributions to the minimum bias rate from the region of small differences in η and ϕ for $p_t^{cut} = 1$ GeV – full trigger response.

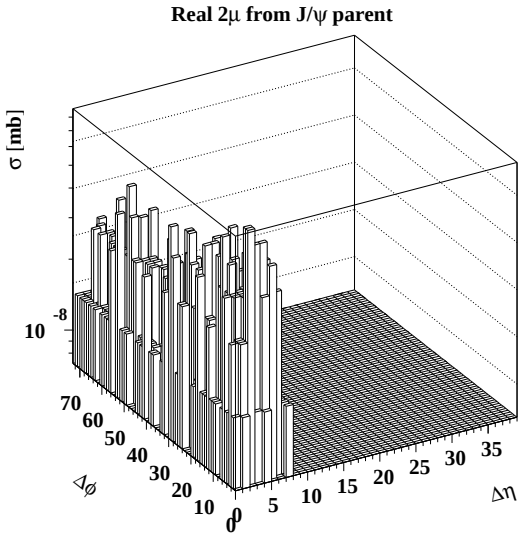

Figure 91: Dependence between $\Delta\eta$ and $\Delta\phi$ for muons from J/ψ in the case of $p_t^{cut} =$ 1 GeV – full trigger response.

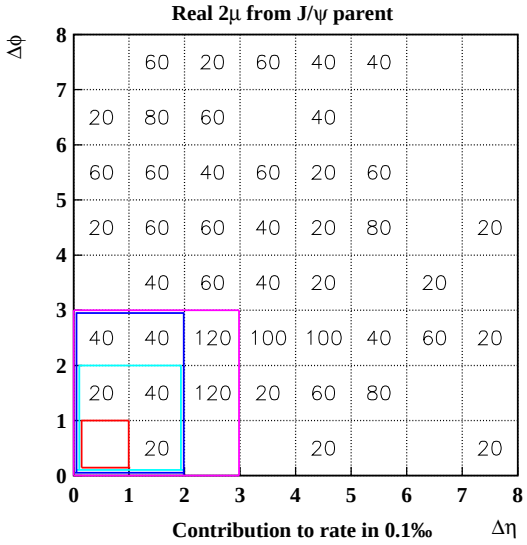

Figure 92: Contributions to J/ψ rate from the region of small differences in η and ϕ for $p_t^{cut} = 1$ GeV – full trigger response.

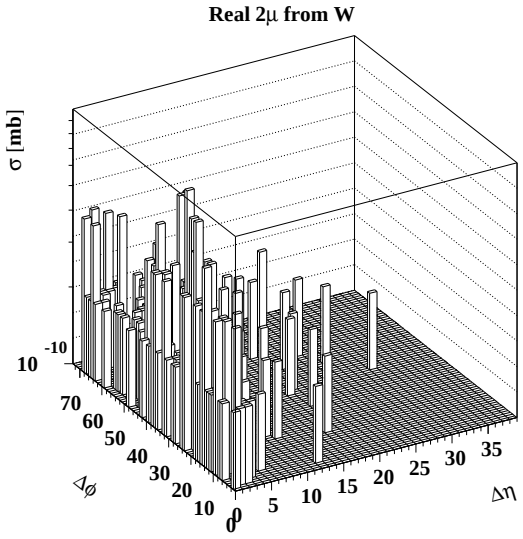

Figure 93: Dependence between $\Delta\eta$ and $\Delta\phi$ for muons from W in the case of $p_t^{cut} =$ 1 GeV – full trigger response.

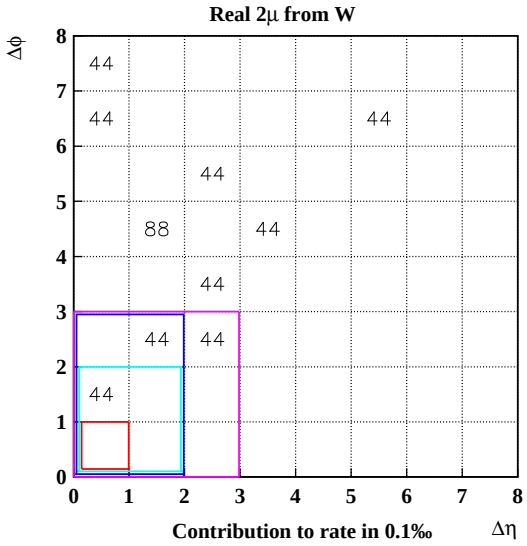

Figure 94: Contributions to W rate from the region of small differences in η and ϕ for $p_t^{cut} = 1$ GeV – full trigger response.

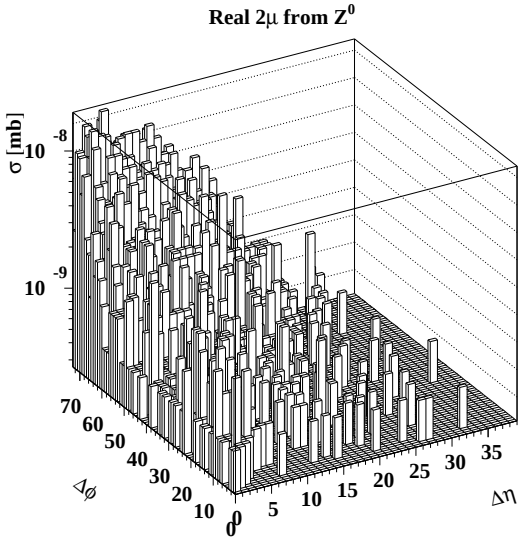

Figure 95: Dependence between $\Delta\eta$ and $\Delta\phi$ for muons from Z^0 in the case of $p_t^{cut} =$ 1 GeV – full trigger response.

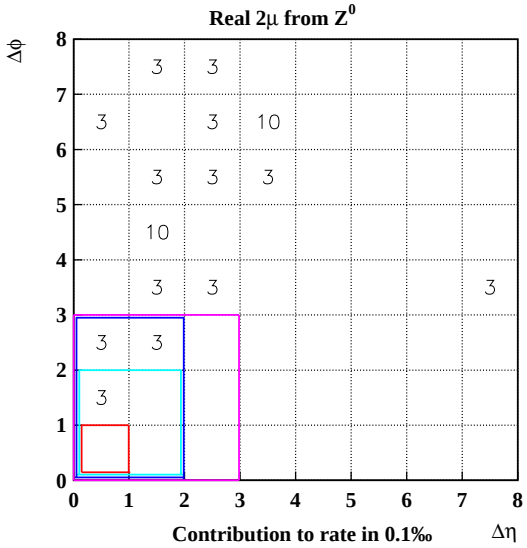

Figure 96: Contributions to Z^0 rate from the region of small differences in η and ϕ for $p_t^{cut} = 1$ GeV – full trigger response.

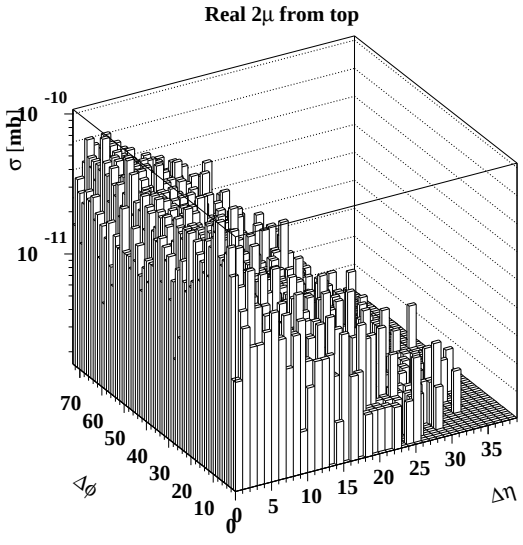

Figure 97: Dependence between $\Delta\eta$ and $\Delta\phi$ for muons from top in the case of $p_t^{cut} =$ 1 GeV – full trigger response.

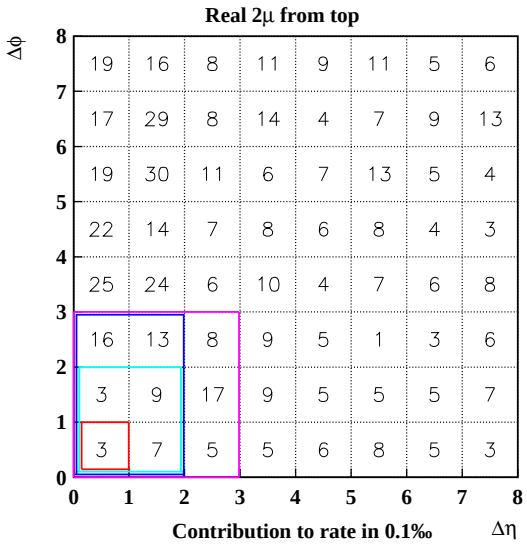

Figure 98: Contributions to top rate from the region of small differences in η and ϕ for $p_t^{cut} = 1$ GeV – full trigger response.

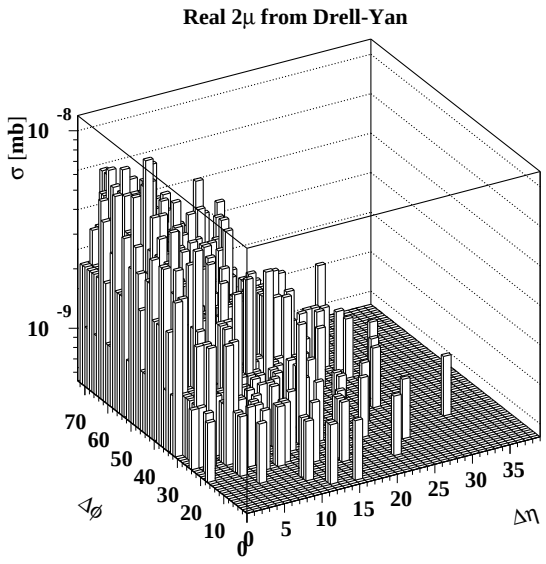

Figure 99: Dependence between $\Delta\eta$ and $\Delta\phi$ for muons from Drell-Yan in the case of $p_t^{cut} = 1$ GeV – full trigger response.

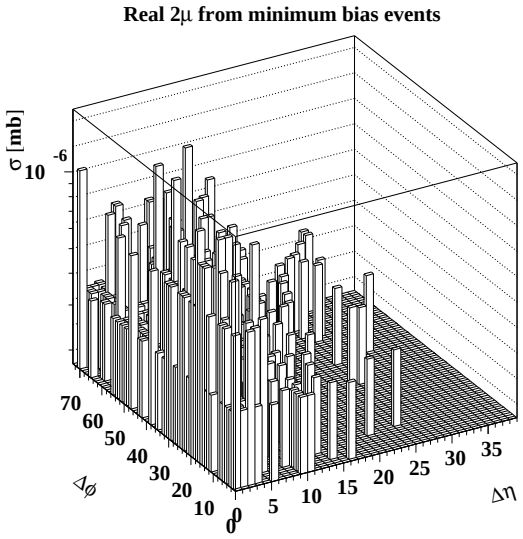

Figure 100: Dependence between $\Delta\eta$ and $\Delta\phi$ for muons from minimum bias events in the case of $p_t^{cut} = 4$ GeV – full trigger response.

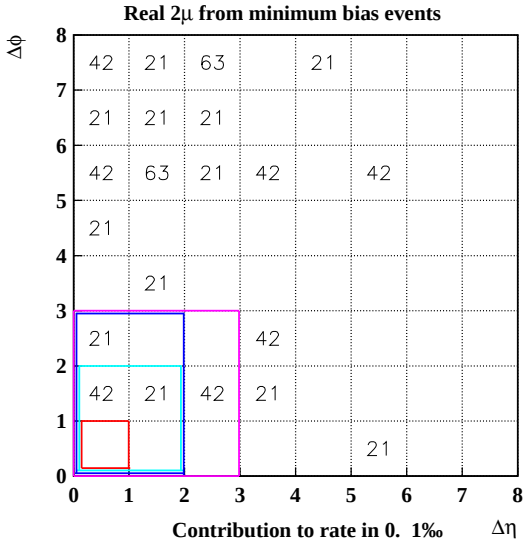

Figure 101: Contributions to the minimum bias rate from the region of small differences in η and ϕ for $p_t^{cut} = 4$ GeV – full trigger response.

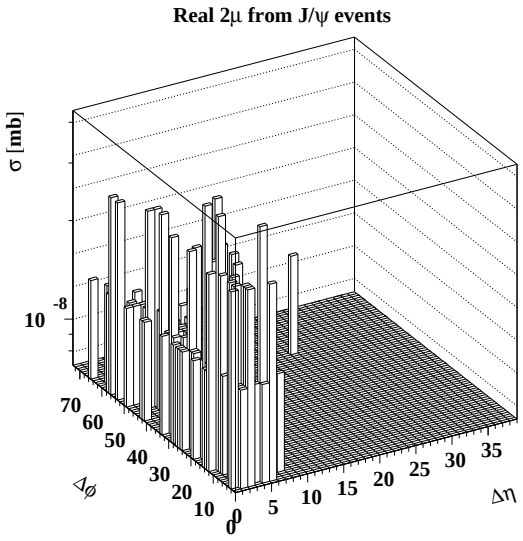

Figure 102: Dependence between $\Delta\,\eta$ and $\Delta\,\phi$ for muons from J/ψ in the case of $p_t^{cut} =$ 4 GeV – full trigger response.

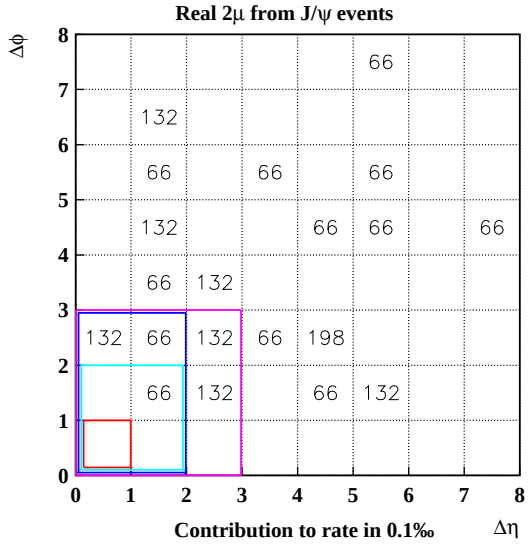

Figure 103: Contributions to J/ψ rate from the region of small differences in η and ϕ for $p_t^{cut} = 4$ GeV – full trigger response.

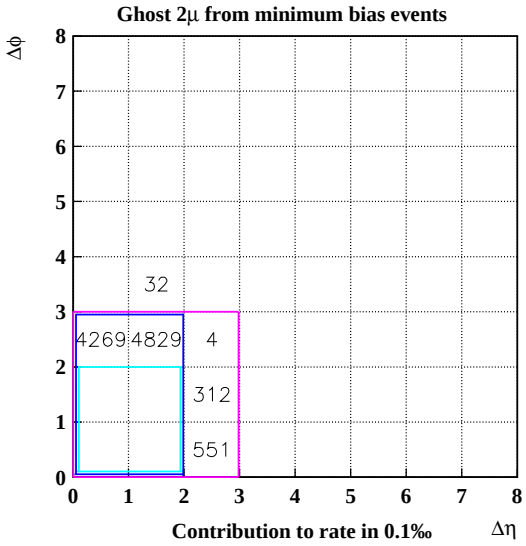

Figure 104: Dependence between $\Delta\,\eta$ and $\Delta\,\phi$ for ghost muons from minbias events in the case of $p_t^{cut} = 1$ GeV

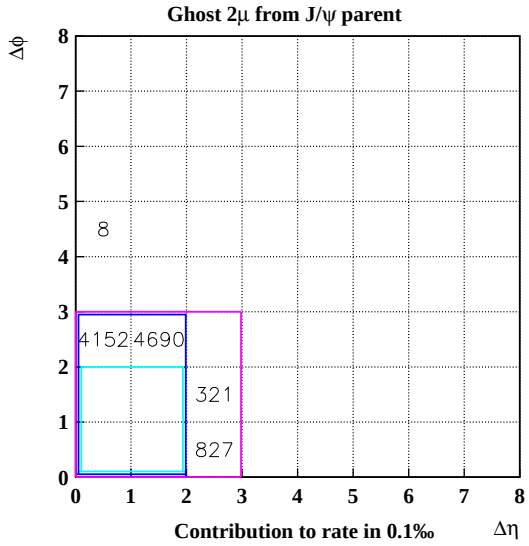

Figure 105: Dependence between $\Delta\,\eta$ and $\Delta\,\phi$ for ghost muons from J/ψ in the case of $p_t^{cut} = 1$ GeV

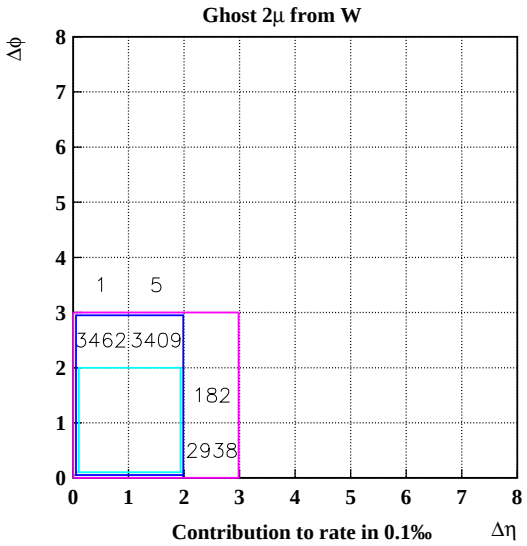

Figure 106: Dependence between $\Delta\eta$ and $\Delta\phi$ for ghost muons from W in the case of $p_t^{cut} = 1$ GeV

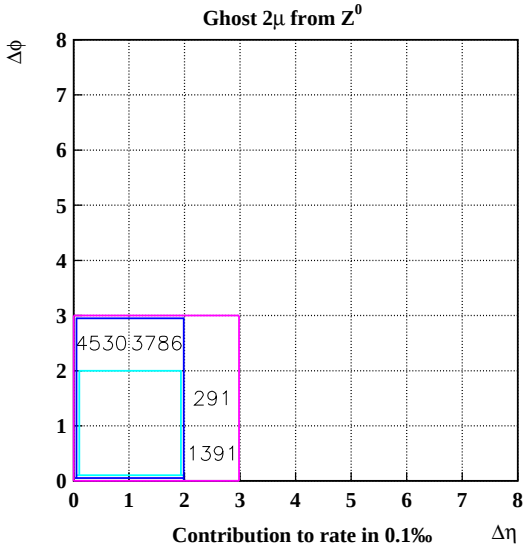

Figure 107: Dependence between $\Delta\eta$ and $\Delta\phi$ for ghost muons from Z^0 in the case of $p_t^{cut} = 1$ GeV

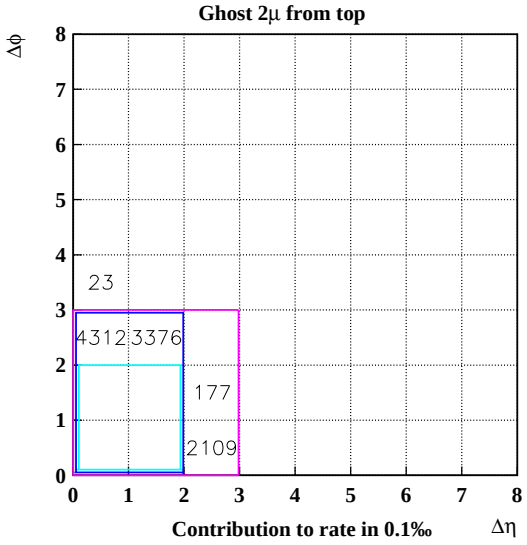

Figure 108: Dependence between $\Delta\eta$ and $\Delta\phi$ for ghost muons from top in the case of $p_t^{cut} = 1$ GeV

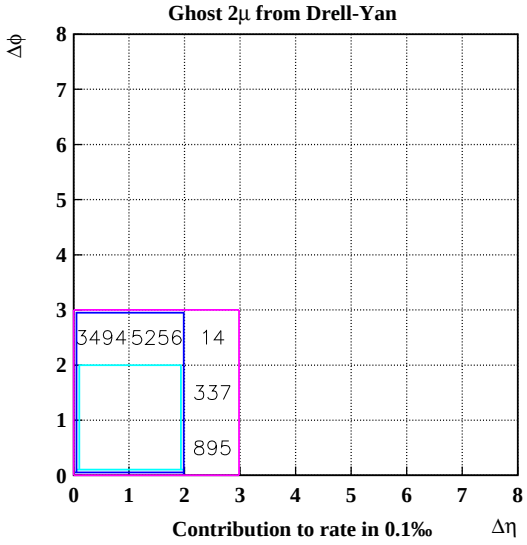

Figure 109: Dependence between $\Delta\eta$ and $\Delta\phi$ for ghost muons from Drell-Yan process in the case of $p_t^{cut} = 1$ GeV

6 Conclusions

The main aims of this thesis, listed in the section 1.6, were achieved and the results are as follows

- Total trigger 2μ rate at 1 GeV will be about 4 kHz, at 4 GeV it will be below 2 kHz. "Magic" value of 100 Hz will be met about 8–10 GeV. In the range of 20 to 50 GeV the rate will decrease from 30 to 10 Hz, and for the highest p_t^{cut}, equal to 100 GeV we will have to deal with about 3 Hz.

- In the small p_t region the rate is dominated by the minimum bias events, whereas above 20 GeV by the Z^0 decays.

- Fake triggers, from superimposing of single μ events, exceed real ones when p_t cut is below $4 - 5$ GeV at the highest luminosity. For higher cuts the dominance of real triggers is achieved. For the highest possible cut of 100 GeV, the ratio "real:fake" is on the level of 50. Fake rate is proportional to L^2 thus at $L = 10^{33}\mathrm{cm}^{-2}\mathrm{s}^{-1}$ the ratio is ten times greater.

- The current algorithm of vetoing embeded in CMSIM101 is insufficient, because it causes more ghosts than proper triggers for the low p_t region. For higher cuts the dominance of the real triggers is achieved.

- The enlargement of the veto area around trigger candidate to two units both in ϕ and η kills more than 99.5 % of the ghosts.

- The price to pay for the enlargement of the veto area is less than 5% loss of 2μ events for all examined types of sources.

The design of the CMS muon trigger – its granularity – seems to suit physics goals. Good efficiency in recognition of 2μ events, crucial for the Higgs detection, is possible to achieve. One should remember that these calculations are based on results of Monte Carlo which predictions may differ from the future experimental results by a factor of two to five.

Acknowledgements

I would like to thank cordially Jan Królikowski for many helpful suggestions, valuable discussions and final revision of this report. I am also very grateful to Marcin Konecki for his support and introduction to CMS software. I appreciate useful comments made by Maciej Górski, Grzegorz Wrochna and Piotr Zalewski. The words of thanks to all members of Warsaw DELPHI and ZEUS groups for wide access to their computers.

7 Appendix A

Types of generations

In order to simulate the main sources of the soft background, for the p-p collisions at $\sqrt{s}$=14 TeV, to the CMS 2 μ trigger, the following processes and PYTHIA parameters were used

- QCD or minimum bias events with the following processes switched on:

  $q_i\ q_j \to q_i\ q_j$
  $q_i\ \overline{q}_i \to q_k\ \overline{q}_k$
  $q_i\ \overline{q}_i \to g\ g$
  $q_i\ g \to q_i\ g$
  $g\ g \to q_i\ \overline{q}_i$
  $g\ g \to g\ g$
  low p_t scattering

  which is obtained with parameter

```
MSEL = 1                          !   minimum bias event
```

- J/ψ production with:

```
MSEL = 0                          !   full user control
```

  $g\ g \to J/\psi\ g$ – MSUB(86)=1
  $g\ g \to \chi_{0c}\ g$ – MSUB(87)=1
  $g\ g \to \chi_{1c}\ g$ – MSUB(88)=1
  $g\ g \to \chi_{2c}\ g$ – MSUB(89)=1

- Single W production with:

```
MSEL = 0
```

  $f_i\ \overline{f}_j \to W^+/W^-$ – MSUB(2)=1
  $f_i\ \overline{f}_j \to g\ W^+/W^-$ – MSUB(16)=1
  $f_i\ \overline{f}_j \to \gamma\ W^+/W^-$ – MSUB(20)=1
  $f_i\ g \to f_j\ W^+/W^-$ – MSUB(31)=1

- Single Z^0 production with:

```
MSEL     =   0
MSTP(43) =   2       !  only Z included from process:
```

$f_i\ \overline{f}_i \to \gamma^*/Z^0$ – MSUB(1)=1
$f_i\ \overline{f}_i \to g\ Z^0$ – MSUB(15)=1
$f_i\ \overline{f}_i \to \gamma\ Z^0$ – MSUB(19)=1
$f_i\ g \to f_i\ Z^0$ – MSUB(30)=1
$g\ g \to Q_k\ \overline{Q}_k\ Z^0$ – MSUB(131)=1

- Drell-Yan process with:

```
MSEL     =   0
MSTP(43) =   1       !  only gamma* included from:
```

$f_i\ \overline{f}_i \to \gamma^*/Z^0$ – MSUB(1)=1

- Top quark production with:

```
MSEL                  =   6     !   top production
PMAS(6,1)             = 174.    !   top mass = 174 GeV
PMAS(LUCOMP(661),1)   = 348.    !
PMAS(LUCOMP(663),1)   = 348.    !
PMAS(LUCOMP(665),1)   = 348.    !   masses of different
PMAS(LUCOMP(10661),1) = 348.    !     theta particles
PMAS(LUCOMP(10663),1) = 348.    !
PMAS(LUCOMP(20663),1) = 348.    !
```

In this case followed processes were automatically switched on:

$f_i\ \overline{f_i} \to Q_k\ \overline{Q}_k$
$g\ g \to Q_k\ \overline{Q}_k$

In this description f_i stands for the fermions, g for the gluons and q_i and Q_i for the quarks. Q_i denotes that the fermion masses are explicitly included in the matrix elements. For all simulations the decay volume for all particles was limited to the cylinder embracing calorimeters which could be made by:

```
MSTJ(22) =    4  ! particle is decayed only within cylinder
PARJ(73) = 2950. ! radius(in xy-plane) expressed in [mm]
PARJ(74) = 5600. ! z extent [-PARJ(74),+PARJ(74)] in [mm]
```

In all mentioned simulations π^0 decays were switched *OFF*[37] and $K^{\pm}$ and $\pi^{\pm}$ decays were left *ON*. π^0 decays were excluded because it does not decay into μ+anything so it is easy way to save CPU time. On the other hand $K^{\pm}$ and $\pi^{\pm}$ are the main source of soft muons[38].

Other switches were preserved with their default values. Distribution of partons in the proton was given by CTEQ2L function – the best leading order fit.

[37] Recipe to switch OFF neutral pion decays – MDCY(LUCOMP(111),1)=0

[38] $\pi^{\pm}$ take about 63% and $K^{\pm}$ about 11% of final state hadrons generated by PYTHIA in minimum bias p-p events at $\sqrt{s} = 14$ TeV. This numbers are based on [11]

8 Appendix B

Tricks used to obtain sufficient statistic

As one can deduce from tables 3 and 4 in section 3 very large statistic was absolutely needed for minimum bias events. The reason was that practically every event in a LHC collision is a minimum bias one, only very few of them produce double μ events satisfying cuts [39]. Additionally, it is expected that minimum bias rate will be decreasing rapidly with increasing p_t cut. To be safe from influence of statistical fluctuations in wide p_t range large statistic becomes necessity.

As one can deduce from the section 2.1 the event evolution in Pythia is divided into three steps:

1. quark–gluon skeleton generation
2. fragmentation–hadronization phase
3. particle decays

Possibility of freezing event on the one of the first two states is given to the user. There are two master switches which governs this:

- MSTJ(1) – responsible for fragmentation scheme

```
= 0 - no jet fragmentation at all
= 1 - string fragmentation according to the Lund model(default)
```

- MSTJ(21) – responsible for particle decays

```
= 0 - all particle decays forbidden
= 1 - unstable particles allowed to decay
```

To make generation of minimum bias events faster division into two phases was applied

1. light particle decays – "K and π events"
2. heavy particle decays – "*beauty* or *charm* events"

It was going according to the schedule:

1. generation of quark–gluon skeleton (hadronization and particle decays forbidden)
2. check if b or c quarks are present

[39] Natural spatial cut on μ momentum direction is $|\eta| \leq 2.4$. Reaching muon stations is possible only for μ with at least $p_t = 1$ GeV/c. It refers to forward region. In the barrel μ has to possess $p_t \geq 3$ GeV/c. Muons with lower p_t do not reach MS because of strong bending in 4T magnetic field and absorption in the calorimeters.

- Yes – save skeleton on disk and generate next one
- No – switch ON jet fragmentation

3. process next part of event generation – Call LUEXEC
   - exclude particle species which do not decay to muons
   - check if $K^{\pm}$ and $\pi^{\pm}$ can give μ with p_t over threshold 1GeV – exclude these which can not – ($\simeq T_{decays}/5$)
4. switch ON particle decays
   - decay the same hadrons in the loop – N times

The repetition factor N=100 was chosen. It should be mentioned that decaying these same particles N times produces biasing of events. Bias was defined as an appearance of the μ pair with exactly same parents at least two times in the same loop. For these conditions[40] biasing of events on the level of 2% was found. But this price is reasonable. Due to time sharing between generation's phases

- **68%** T_{gen} – quark-gluon skeleton generation
- **29%** T_{gen} – jet fragmentation
- **3%** T_{gen} – particle decays

simulation of so called "K and π events" was shorter **25 times** than it would be without repetitive decays.

Decay of saved "*beauty* and *charm* skeletons" was done in a separate job. In this case loop–decays (also $\times 100$) were performed from the parton level. The reason lies in danger of significant bias of the sample due to relatively big branching ratios for B, D mesons going into μ + anything[41]. When hadronization was done for every event from the begging, the decays of exactly the same set of hadrons were impossible so the probability of sample bias was lower. Of course exclusion of particles, mentioned above, had not much sense in this case. So proportions between phases has changed:

- **60%** T'_{gen} – quark-gluon skeleton generation[42]
- **25%** T'_{gen} – jet fragmentation
- **15%** T'_{gen} – particle decays

[40] Decay volume $|z| \leq 5600$ mm, $r \leq 2950$ mm

[41] For some mesons $\simeq 10\%$

[42] Naturally it was not performed once again.

It could seem that profit is only about 2.5 shortening of the generation time but taking into account that one "b,c event" happens per 15 minimum bias events we obtain **30 times** profit.
It should be stressed that normalisation to correct number of events should be performed:

$$N_{events} = 100 \times N_{skeletons}$$

Another possibility of shortening generation time was used in J/ψ events generation. All decay channels except $J/\psi \to \mu^+\mu^-$ were switched OFF. Recipe for this is shown in form of the following Fortran code:

```
      KC=LUCOMP(443)
      Do i=MDCY(KC,2),MDCY(KC,2)+MDCY(KC,3)-1
        If( (IABS(KFDP(i,1)).Ne.13).Or.
     +      (IABS(KFDP(i,2)).Ne.13).Or.
     +      (IABS(KFDP(i,3)).Ne.0) ) MDME(i,1)=0
      EndDo
```

Explanation:

- KC=LUCOMP(443) – to give the compressed particle code for J/ψ
- MDCY(KC,2) – entry point into decay channel table for particle with compressed code KC
- MDCY(KC,3) – total number of decay channels for particle with compressed code KC
- KFDP(IDC,j) – contain the decay products for channel IDC
- MDME(IDC,1) – to switch ON (1) or OFF (0) individual decay channel IDC

Normalisation is done to:

$$N_{events} = N_{gen} \times \frac{1}{BR(J/\psi \to \mu\mu)}$$

Generation has taken about 2500 CPU hours on SGI workstations[43]. Minimum bias simulation has consumed about 85% of this. It should be stressed that without mentioned manipulations these studies have not been possible at all.

[43] SGI cluster of Warsaw University Particle Physics Division consists of 8 machines with 100MHz and 150MHz clocks

References

[1] J.D.Jackson *Classical Electrodynamics*, PWN, Warszawa 1982

[2] *Particle Physics Booklet*, Particle Data Group, July 1994

[3] *The Large Hadron Collider - Conceptual Design*, CERN/AC 95-05, 20 October 1995

[4] *The Compact Muon Solenoid - Technical Proposal*, CERN/LHCC 94-38, 15 December 1994

[5] T. Sjöstrand, *PYTHIA 5.7 and JETSET 7.4 - Physics and Manual*, CERN-TH.7112/93, December 1993, (revised August 1994)

[6] *LHC Workshop*, Proceedings Vol I–III, Aachen , 4-9 October 1990

[7] M. Konecki, J. Królikowski, G. Wrochna, *Simulation Study of the RPC based, single muon Trigger for CMS* CMS TN/92-39, September 1992

[8] M. Konecki, J. Królikowski, I. M. Kudla, G. Wrochna, *RPC geometry and Muon Trigger acceptance* CMS TN/95-120, 4 September 1995

[9] M. Adlinger et al., *Pattern Comparator Trigger (PACT) for the Muon System of the CMS experiment* CERN-PPE/94-227, 9 December 1994

[10] R.Loddo et al., *CMS Muon Trigger Preliminary specifications of the baseline trigger algorithms* CMS TN/96-060, 17 February 1996

[11] M.Ćwiok, G.Wrochna, *Muon rates in UA1, D0, CDF and CMS predicted by PYTHIA 5.7*, CMS TN/95-150, 23 October 1995

[12] M. Konecki, J. Królikowski, G. Wrochna, *RPC Muon Trigger Software MRPC 100 – 102*, CMS technical note in preparation,
`http://cmsdoc.cern.ch/~wrochna/mrpc/mrpc.ps`